Geomorphic Mapping and Ground-Penetrating Radar Survey of the Agua Blanca Fault in Valle de Santo Tomas, Baja California, Mexico

By

William Rainey Cage

Bachelor of Science, 2008
Texas Christian University

Submitted to the Graduate Faculty of
The College of Science and Engineering
Texas Christian University
In partial fulfillment of the requirements
For the degree of

MASTER OF SCIENCE

August 2010

Acknowledgements

First and foremost, I would like to thank my direct advisor, Dr. Helge Alsleben, for his insight in the field, the countless hours he spent assisting me with my work, and his endless patience (as much was needed). I sincerely appreciate the time and effort he gave me as I always felt he kept my work a priority despite his busy schedule. I am also indebted to my other committee members, Dr. Arthur Busbey and Ms. Morgan, for their time and knowledge contributed to this study. A special thanks to Juan Pablo Nuñez and Antonio Baro, of the beautiful Santo Tomas Vineyard, for allowing us access to the property. I gratefully thank my field assistants, John Munoz and Alan Ruiz, for help translating with the locals and hours of machete work in the hot Baja sun, without whom I might still be hacking at brush on the hillside avoiding snakebites. The dedication of a month of their summer break was much appreciated and hopefully allowed them to carry away as many positive memories as I did from our time spent in Mexico. The Gonzalez family showed us great hospitality during our stay and the delicious paella will not be soon forgotten. Codie Kretzer provided an enormous amount of aid and deserves much credit for deciphering and teaching me how to use the EKKO_View software. Without his "how to" packet I might still be staring helplessly at a computer screen. I would also like to thank Dave McCleery, Matt Koehler, and Rhett Heartsill - a great group of friends whose moral support and daily lunches the past few years has helped alleviate the stress of writing a thesis. Finally, this undertaking would not have been possible without the encouragement and support of my parents in all my endeavors. To them I simply say thank you for everything.

Table of Contents

List of Figures

List of Tables

List of Plates

Chapter 1: Introduction

1.1   Statement of Problem

A better understanding of the near-surface character of active strike-slip faults and their overall three-dimensional structural characteristics is desirable in order to better understand the complexities of faulting that may not be directly visible at the surface. However, besides labor-intensive trenching studies and expensive efforts to drill into these faults, getting a clear image of the nature of these structures in the near-surface can be difficult. To help our understanding of strike-slip faults, the Agua Blanca fault in northern Baja California, Mexico, is chosen for study (Figure 1).

The study area of the fault is in the Valle Santo Tomas (Figure 2). Mapping completed in the area shows the geomorphology and physiographic features that provide evidence for recent faulting. In addition to surface mapping, a detailed ground penetrating radar (GPR) survey, which is a rather new geophysical technique for geologic investigations, of the fault was completed. By combining surface mapping and a detailed GPR survey of the fault, the geometry of the active strike-slip fault is much better visualized and understood. Ultimately, the information gained in this study will help aid in understanding the role of the fault and its relationship to the San Andreas fault system.

1.2   Introduction to the Agua Blanca fault

The Agua Blanca fault, which is interpreted as an active, dextral strike-slip fault in northern Baja California about 100 km south from the U.S.-Mexico border (Rockwell *et al*., 1993; Dixon *et al*., 2002), is the target for the present study. Tectonically, the Agua Blanca fault
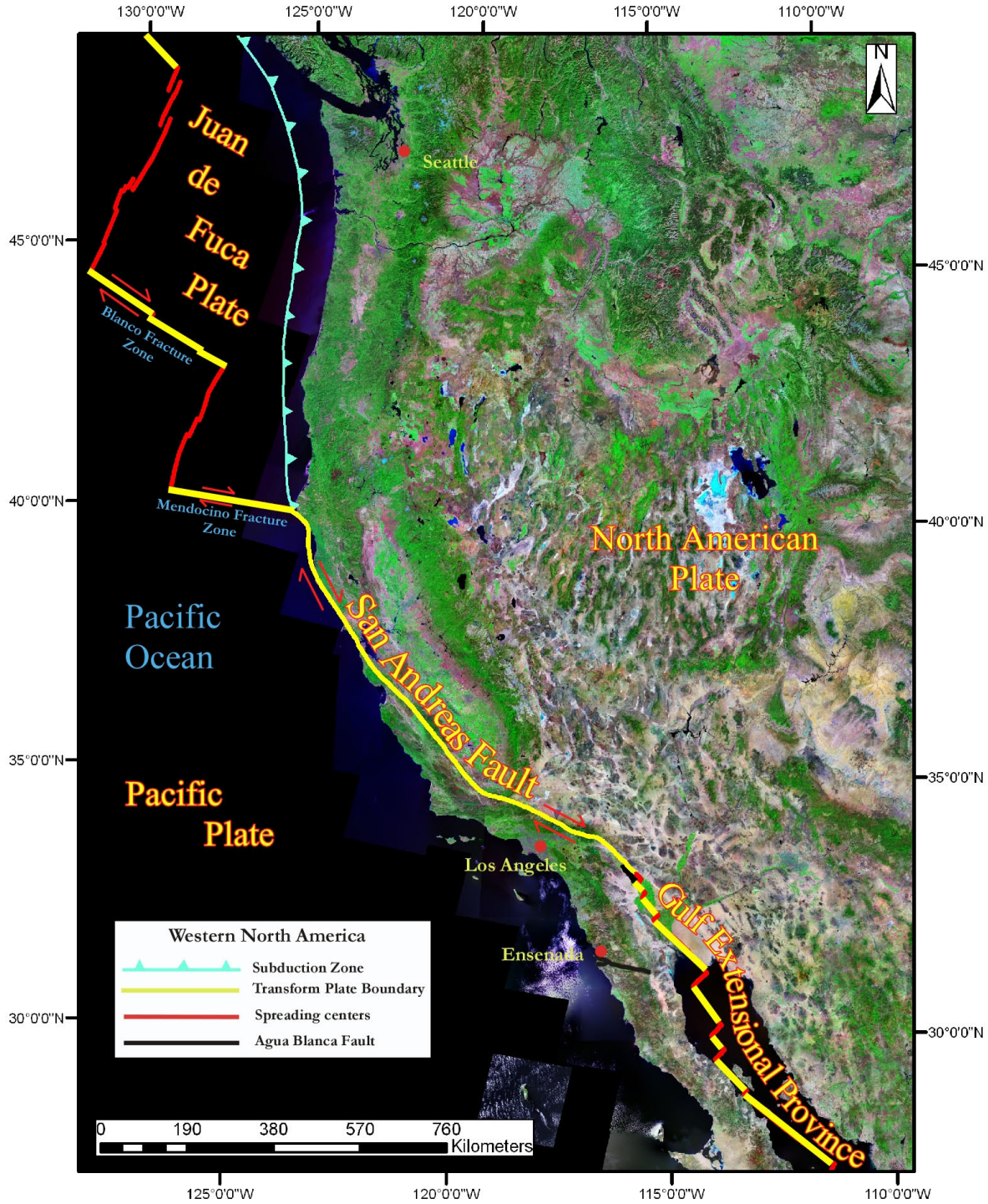
Figure 1. Tectonic setting of western North America including the San Andreas fault (Modified from Kretzer, 2010).

Figure 2. Modified Google Earth image showing the location of the Agua Blanca fault on the North American continent. The inset is a close-up view of the fault and the yellow box represents the study area.

is associated with the San Andreas fault system, which comprises the main portion of the transform plate boundary between the Pacific and North American plates (Figure 1). The Agua Blanca fault is ~120-km-long and is generally divided into three major right-stepping segments that run transversely across the Baja Peninsula (Figures 2 and 3; Rockwell *et al.*, 1987; 1993). Each segment is ~40 km in length with a trend ~30º counterclockwise to the more northwesterly trend of the San Andreas fault system (Allen *et al.*, 1960; Rockwell *et al.*, 1987; 1993).

A limited number of studies on the Agua Blanca fault suggest Quaternary fault activity with estimated slip rates between 4 and 8 mm/yr (Rockwell *et al.*, 1987, 1993; Dixon *et al.*, 2002). Rockwell *et al.* (1987, 1993) conducted trenching studies, while Dixon *et al.* (2002) used campaign GPS data in order to provide information on slip rates and Quaternary neotectonics for the Agua Blanca fault. Dixon *et al.* (2002) conclude that the Agua Blanca fault is active and that, despite its unusual orientation, the fault should not be considered an abandoned fault. The fault is most likely locked and accumulating strain, which will result in an earthquake in the future (Dixon *et al.*, 2002). Although there are estimated slip rates for the fault, there is no recorded seismicity. This lack of seismic activity is of potential concern because the city of Ensenada with its population of ~250,000 is located within 15 km of the fault (Figure 2). The city is primarily constructed from unreinforced masonry buildings and any substantial seismic activity could be devastating.

1.3 Geomorphic Features Associated with Active Tectonism

In active tectonic regions where strike-slip faulting is dominant, a number of geomorphic features are commonly associated with the motion and deformation in the vicinity of the fault. The most distinctive characteristic of strike-slip faults is their overall structural linearity
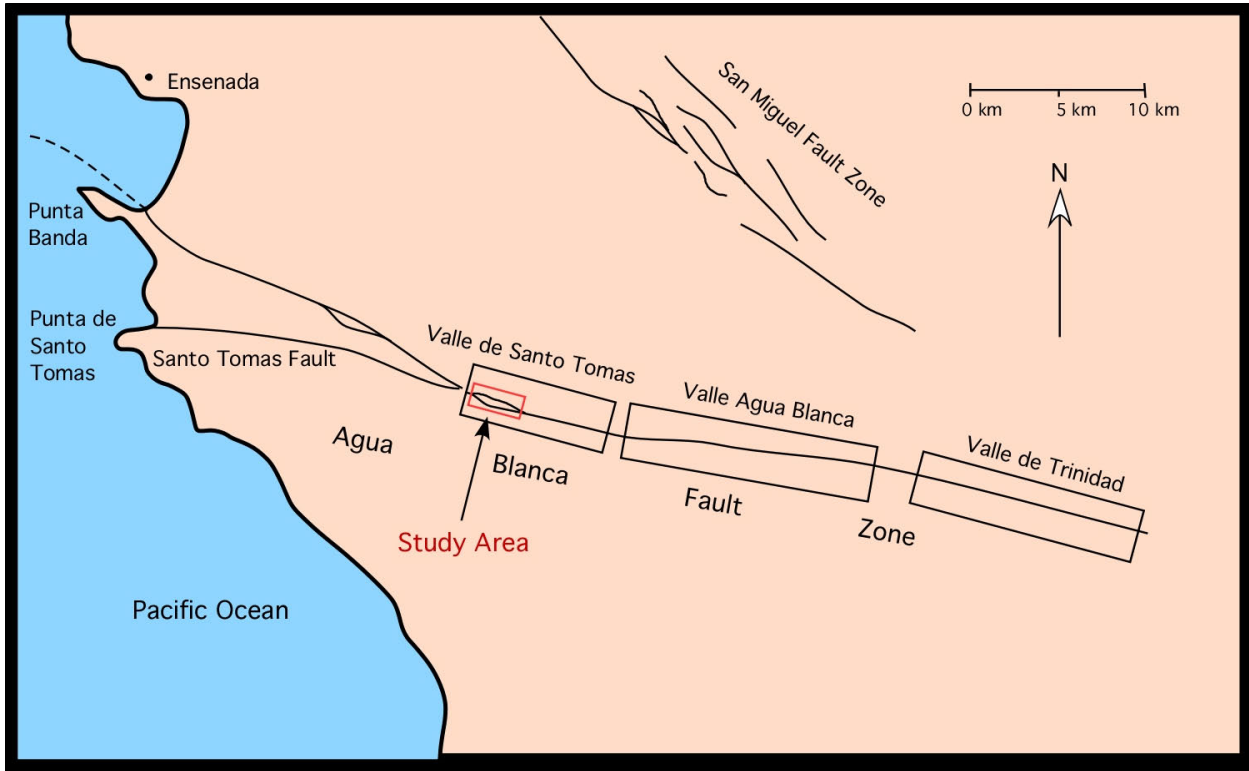
Figure 3. Main trace of the Agua Blanca fault. Red box shows general location of the study area in the Valle Santo Tomas. Larger black boxes show general locations of valleys along the fault with corresponding names above. (Modified from Suarez-Vidal *et al.,* 1991)

over long distances (Sylvester, 1988). Other physiographic features indicative of strike-slip faulting include scarplets, deflected streams, pressure ridges, sag ponds, and shutter ridges (Figure 4; Sylvester, 1988). However, the preservation potential of many of these landforms is highly dependent on climate and rapid erosion is possible. Thus, these geomorphic features have a finite life expectancy and may not always be present, even if the fault is still active.

Shutter ridges and scarplets can form when a topographic high is adjacent to a topographic low. This may occur during strike-slip faulting when lateral movement along the fault dissects a hill and each side of the dissected hill is subsequently moved apart. The translation of the adjacent supporting landform can create sudden topographic relief from a high to a low on opposite sides of the fault. Over time, the steep faces weather and erode and piles of sediment form as a result of slope failures (Sylvester, 1988). If truncation of ridge and canyon topography occurs and a ridge is translated so that it blocks the flow of water or shuts off a canyon, the lateral displacement on the fault can cause the formation of a shutter ridge (Figure 4, e.g., Sylvester, 1988).

Deflected stream channels occur when a fault line intersects an active stream. When a stream originally encounters a fault zone, it may cut strait across the fault. Episodic lateral movement along the fault will deflect the streams, which tend to erode along the fault trace and make a 90˚ turn until encountering the lower, offset part of the stream channel. When the offset stream channel is encountered, the stream will make another 90˚ turn and continue along its natural path downslope. Deflected streams are good indicators to establish the direction and amount of relative lateral displacement along a fault, but must be used with caution. The lateral offsets must be analyzed in a stream that travels down a moderate slope and intersects the fault at a right angle in order to be trusted for measuring fault displacement. If a stream is traveling along
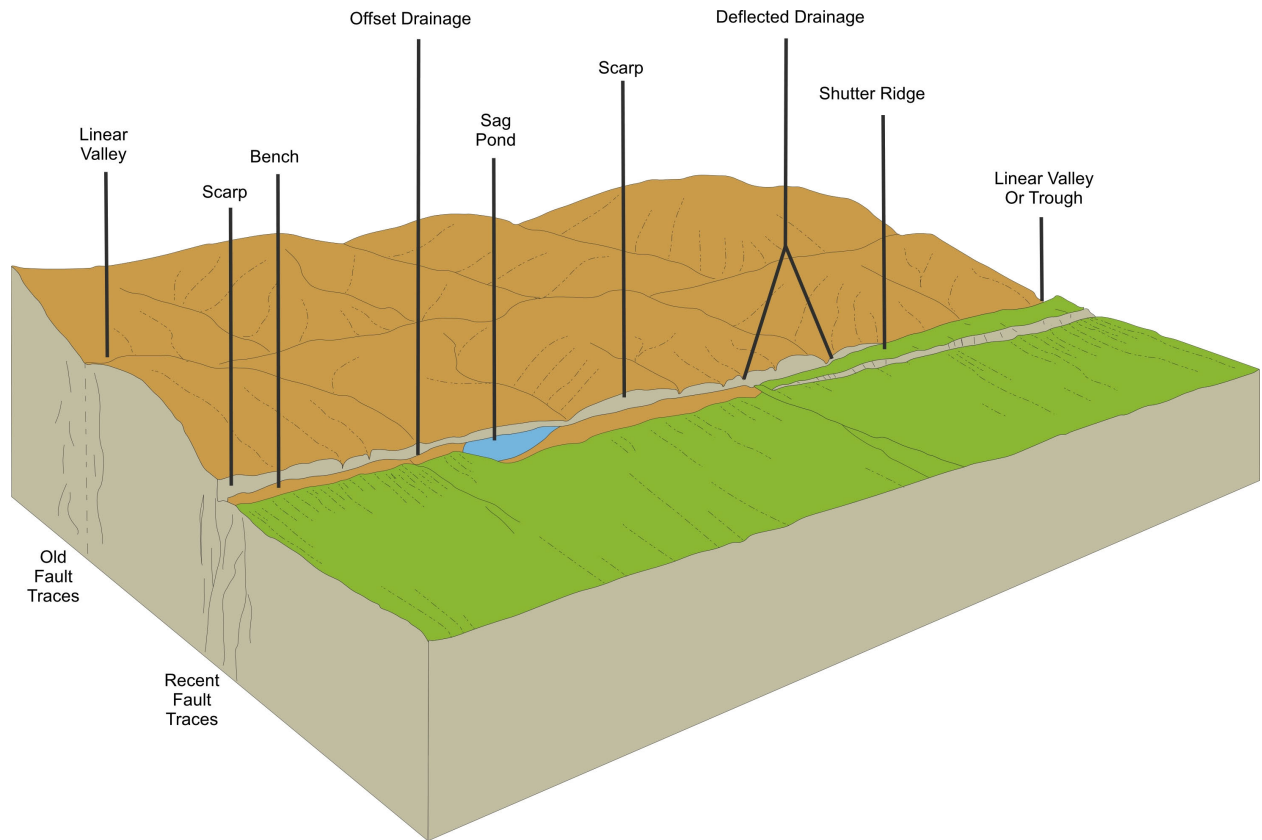
Figure 4. Geomorphic structures associated with strike-slip faults (From Kretzer, 2010).

a gentler gradient, the water may find the fault trace to be the least resistant natural path and travel along the structural trough for some distance before turning downslope. Thus, differential erosion may be used to explain apparent offsets rather than direction of movement along the fault (Sylvester, 1988).

Identification of several other features can support fault activity. Fault breccias and gouge, which represent broken and crushed rocks caused by faulting, may become visible along fault parallel trenches or troughs created by increased incision in these weaker, crushed, and often poorly lithified zones. Furthermore, small bends in a strike-slip fault can create pressure ridges in a restraining bend where compression occurs between the two fault blocks. These bends cause the fault blocks to converge at an oblique angle rather than move in a transcurrent motion. Many times pressure ridges are created when small blocks or slivers left between the two main opposing blocks of the fault zone rise, tilt, or slide obliquely to the transverse motion of the fault movement and are uplifted. In contrast, sag-ponds are created in a releasing bend when blocks subside through downward tilting or create a sag where a bend in the fault creates a depression after movement (Figure 4, e.g., Sylvester, 1988).

1.4 Ground-Penetrating Radar

While mapping remains an essential part of most geologic studies, ground-penetrating radar (GPR) is a rather new technology and its application to geology is in its early stages (Cai *et al.,* 1996). GPR is an electromagnetic method that provides data similar to seismic reflection data. While seismic profiles are a consequence of spatial distribution of elastic properties of the Earth, features evident in GPR profiles result from the spatial distribution of electrical properties (Cai *et al.,* 1996).

The equipment for the GPR system includes a control unit that can be carried on the back, transmitting and receiving antennas connected to the control unit through fiber optic cables, and a digital video logger (DVL) to view the readings. The transmitting antenna on the surface sends a high frequency (1-1000 MHz) electric wave pulse into the ground where radar waves are refracted when moving from one medium to another (Cai *et al.,* 1996). Frequencies of 100 and 50 MHz have been most successful in obtaining the best images of faults from both shallow (~5 m) and deeper (~20 m) levels, respectively (Slater and Niemi, 2003). Some of the high frequency waves are reflected off of different stratigraphic and structural boundaries and travel back to the surface. The receiving antenna records the time interval between sending and receiving these signals (Figure 5). The difference in arrival times from one emitted electric wave pulse represents the additional time needed for the signal to reach different mediums that may be farther from the transmitter. The signals that arrive back at the receiver first represent the shallower mediums, and as the time interval increases between sending and receiving the signal, the stratigraphic or structural boundaries become progressively deeper. The recorded signals are then sent to the control unit, amplified, digitized and displayed on the DVL where the orientation and location of fault structures can be recognized by linear termination and symmetrical offset of stratigraphic boundaries (Wallace *et al.,* 2010).

Electromagnetic waves travel through different mediums at different velocities. The energy reflected back to the receiver from different interfaces is caused by the change in propagation velocity as energy passes from one stratigraphic or structural feature to the next (Cai *et al.,* 1996). Propagation velocity of electromagnetic waves decreases as the dielectric permittivity increases. Dielectric permittivity is a measure of the potential of a material to store
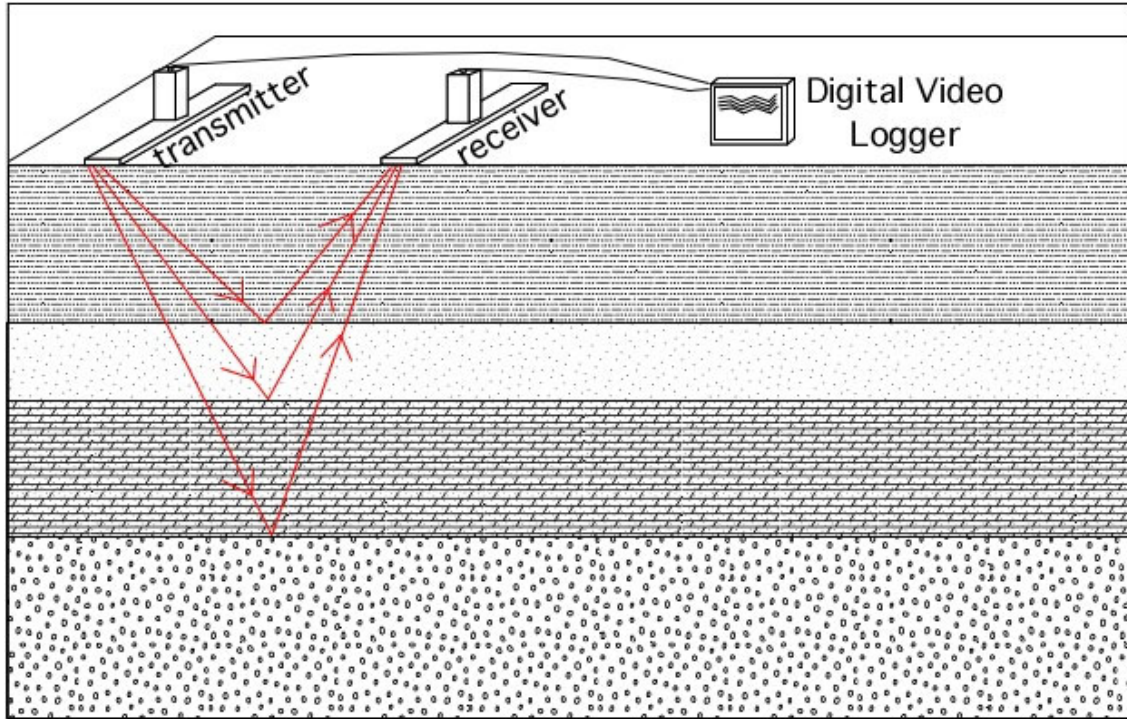
Figure 5. Schematic drawing showing electromagnetic waves reflecting off strata and being recorded by GPR unit (From Madsen, 2009).

an electrical charge when an electric field is applied (Cai *et al.,* 1996). Therefore, a material that has high electrical conductivity will result in energy flowing through the material rather than being reflected off of it. The attenuation of GPR waves in this environment removes energy from the system so that returning reflections from the subsurface become weak and are unable to be accurately recorded by the receiving antenna. Thus, if the materials in the area under investigation have a high dielectric permittivity, the results may be poor (Cai *et al.,* 1996). Earth materials have a dielectric permittivity greater than that of air (0.3 m/ns), so the propagation velocity in the earth will be less than that of air. Because these earth materials vary in conductivity, the depth axis must be calibrated based on the type of rock through which the GPR signal is transmitted (Table 1) (Tischler *et al.,* 2002).

The quality of GPR data is strongly dependent on the geologic environment. Where sedimentary deposition results in well-layered sequences, the GPR reading typically shows many near horizontal features that correspond to changing strata. Well-layered sequences make it easier to identify features such as offsets in the continuity of the strata in the subsurface (Slater and Niemi, 2003). Clay-dominated areas commonly give poor readings due to higher electrical conductivity of the clays, while unconsolidated sands and gravels typically show better results (Cai *et al.,* 1996). A wet environment is not conducive to GPR and increases the dielectric permittivity of the soil, causing the attenuation of transmitted energy. Therefore, it is best to conduct GPR surveys under the driest conditions possible in order to reduce attenuation and maximize the depth of penetration.

Table 1. Typical Wave Propagation Velocities of Common Materials (from Sensors & Software Inc. PulseEKKO® 100 GPR manual)

Material	Velocity (m/ns)	Attenuation (dB/m)
Air	0.3	0
Ice	0.16-0.17	0.01
Dry soil	0.15	
Dry sand	0.15	0.01
Granite	0.13	0.01-0.1
Dry salt	0.13	0.01-0.1
Dry rock	0.12	
Limestone	0.12	0.4-1.0
Wet rock	0.1	

Material	Velocity (m/ns)	Attenuation (dB/m)
Concrete	0.08-0.12	
Pavement	0.1	
Shale's	0.09	1-100
Silts	0.07	1-100
Wet soil	0.06	
Wet sand	0.06	0.03-0.3
Clays	0.06	1-300
Fresh water	0.033	0.1
Sea water	0.033	1000

Changes in magnetic properties and porosity will also affect wave velocity and attenuation (Cai *et al.*, 1996). In order to leave the electric field as undisturbed as possible during the survey, it is important to avoid any metal objects (e.g., powerlines, wire fences, buried pipes) including those that may be carried by the surveyors (e.g., shoelace eyes on boots, belts, handlens, hammer). Zones of high porosity may be less conductive for electric waves as there is less dense material to pass through, while very tight or well-consolidated zones may pass energy with ease. In a desert environment, high salt content along the surface due to intense evaporation of surface water could result in high subsurface electrical conductivity, which may limit electromagnetic wave propagation (Slater and Niemi, 2003).

Resolution of subsurface features and depth of penetration are also very important factors in GPR surveys. Much as seismic surveys, there is generally a tradeoff between these two factors. The higher the frequency emitted by the transmitting antenna, the higher the resolution of subsurface features will be. However, this will result in less depth penetration. Conversely, the lower the frequency transmitted the lower the resolution becomes to distinguish between features. As expected, this also results in greater depth penetration. Therefore, the frequency and antenna size used in GPR surveys should have a good balance of resolution and depth penetration based on the objectives of the study.

In order to obtain a value for depth calibration that is more accurate for a particular area of study than the values shown in Table 1, a common mid-point (CMP) survey may be performed. In this survey method, the antennas are placed a set distance apart from a central point. After the survey is started, the antennas are moved step-by-step at a specified distance in opposite directions from one another sending and receiving signals after every step. Using the known distances between the antennas after each reading and the differences in travel time, a

CMP survey allows calculation of the best propagation velocity to use based on the unique lithology of the area (Figure 6A, e.g., Yetton and Nobes, 1998).

When collecting an image of the subsurface along a line, a reflection survey is most appropriate (Figure 6B). In this survey type, antennas are moved along a line and are separated by a constant distance. This means both the transmitter and receiver are moved an equal distance in the same direction. The signals that are recorded can be stacked, viewed and interpreted on the DVL. After being recorded and stored on the DVL, the data can be post-processed in order to accentuate the resolution and reduce noise present in the raw data.

Chapter 2: Geologic Background

2.1 Tectonic Evolution of the North American Plate Boundary System

The Agua Blanca fault is spatially associated with the San Andreas fault system, which is part of the Pacific-North American transform plate boundary. This system formed as a result of interactions between the Pacific and North American plates during the Cenozoic (Atwater, 1989). However, before these two plates began to interact with one another only ~30 mya, the now largely consumed Farallon plate was being subducted beneath the North American plate at a rate of 7-10 cm/yr (Atwater, 1989; Figure 7). At the same time, a mid-ocean ridge system, which separated the Farallon plate from the Pacific plate, was spreading at a rate of 5 cm/yr (Atwater, 1989). The discrepancy between these two rates caused the migration of the East Pacific Rise towards the subduction zone in North America (Atwater, 1989). Production of oceanic crust along the East Pacific Rise and subduction of the Farallon plate beneath North America is likely
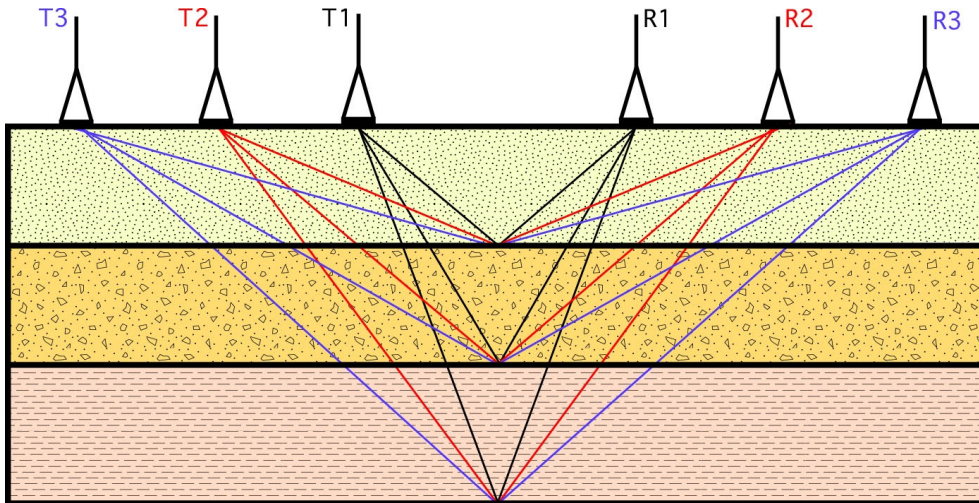
A. Common Mid-point Survey (CMP)
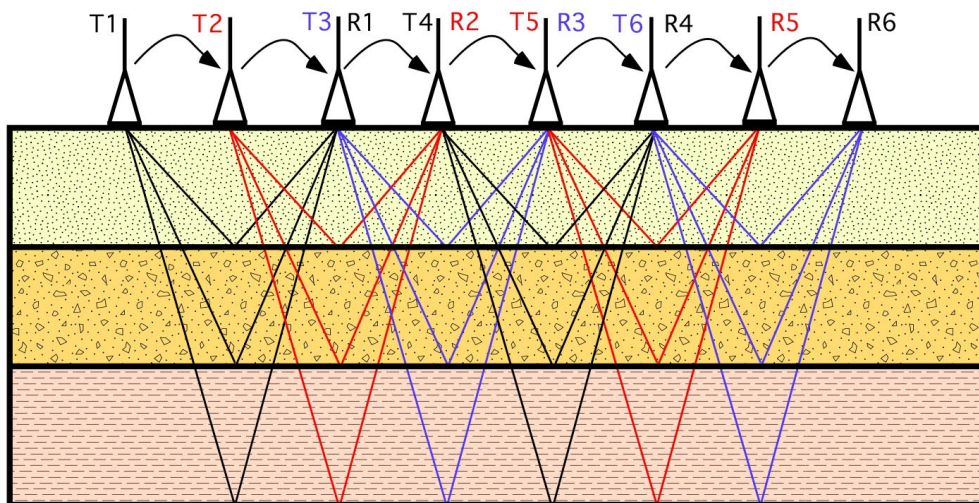
B. Reflection Survey

Figure 6. A. Common mid-point survey. B. Reflection survey. In both surveys T1 marks location of first transmission and R1 is first location of the receiver. Transmitter and receiver are then moved to the next location indicated by the increase in numbers before the next reading is taken.

long-lived. This is supported by the age of the Pacific Ocean floor. The data show that the age of the ocean floor becomes older as you move westward away from the Pacific-North American plate boundary (Atwater, 1970). Since magnetic isochron dating on the ocean floor suggests that spreading centers generally produce oceanic crust at roughly the same rate on either side of a ridge (Stock and Molnar, 1988), the symmetrical counterpart to the current oceanic crust that makes up the Pacific plate on the east side of the spreading centers (the Farallon plate) must have been consumed in a trench.

A central section of the East Pacific Rise between the Mendocino and Murray fracture zones was farther east than other ridge segments (Figure 8) and, therefore, was the first to reach the trench ~ 30 mya near today's latitude of Los Angeles (Dickinson *et al.*, 2005). When the mid-ocean ridge reached the subduction zone, the Farallon plate split into two separate plates; the Vancouver plate, which was the predecessor to the modern Juan de Fuca plate, to the north and the Cocos plate to the south (Atwater and Stock, 1998). The result was an unstable quadruple junction (e.g., Kearey et al., 2009) that immediately devolved into one ridge-trench-transform triple junction and one trench-transform-transform triple junction. The northern junction evolved between the North American, Vancouver, and Pacific plates (Mendocino triple junction), and the southern junction between the Cocos, North American, and Pacific plates (Rivera triple junction) (Dickinson *et al.,* 2005).
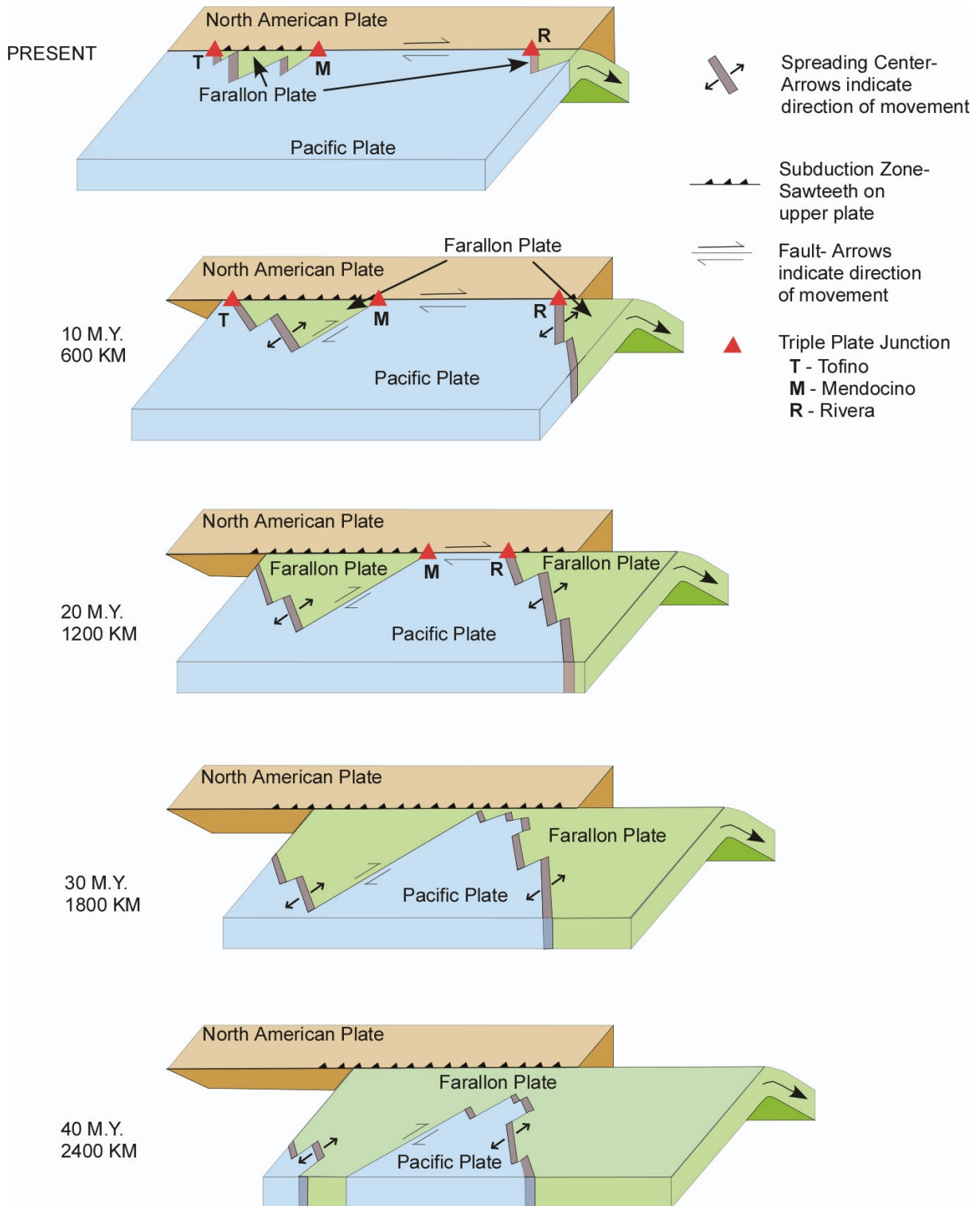
Figure 7. Evolution of the Pacific-North American plate boundary. Redrawn from Irwin (1990)
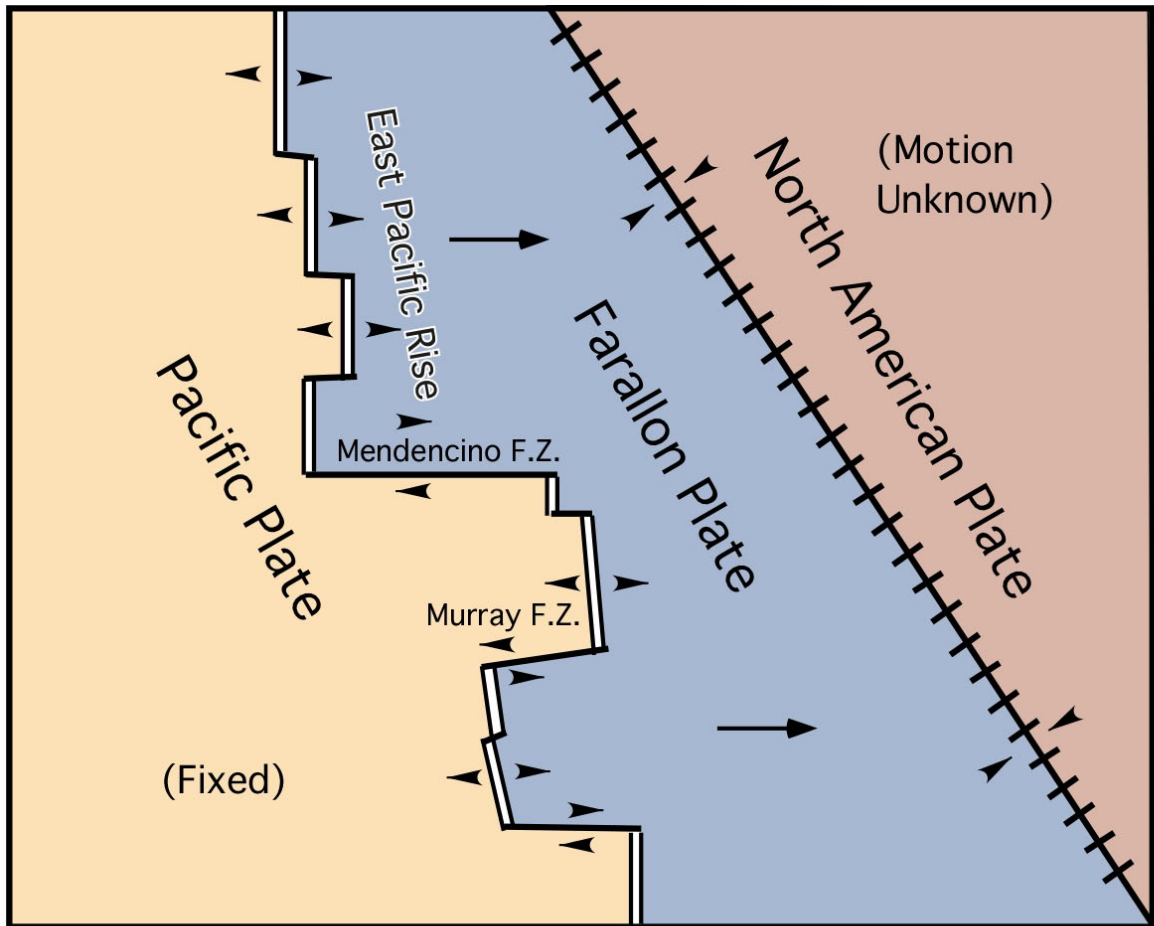
Figure 8. Configuration of plate boundaries 53 mya before Pacific-North American plate interaction. Single lines are transform faults; double lines are spreading centers, Hatched line is subduction zone. Large arrows show direction of relative plate movement. (Modified from Atwater, 1970)

As soon as the quadruple junction formed, the Pacific plate and the North American plate came into direct contact. The relative motion between these two plates resulted in a right-lateral strike-slip fault and transform faulting replaced the subduction zone in the area (Irwin, 1990). As plate motions continued and the Vancouver and Cocos plates continued to be consumed in the trench, the two evolving triple junctions began to migrate apart from one another, which resulted in a continuously growing transform fault system and caused volcanism to cease in the region (Figure 9; Irwin, 1990).

While the transform boundary was still young, motion between the North American and Pacific plates was accommodated in the Continental Borderland along the continental margin because the oceanic crust was young, hot, and easily deformable (Atwater, 1989; Dickinson, 1996). After a cooling period of 5-7 Ma, the borderland became more rigid and most of its ability to take up motion between the two plates was lost (Atwater, 1970). Motion was increasingly transferred to inland faults including the Walker Lane, San Andreas, and Eastern California shear zone (Figure 10), all of which accommodate portions of the total deformation (Atwater, 1970; Dickinson, 1996). Initial movement along the San Andreas fault proper is thought to have originated from 18 to 12 mya (Atwater, 1970; Dickinson, 1996).

In the current configuration, most of the modern plate motion between the North American and Pacific plates is taken up by the San Andreas fault system and the Walker Lane fault system (Figure 10), while some of the motion may be accommodated by deformation in the Basin and Range Province (Wesnousky, 2005). In order to compensate for bends along the San Andreas fault that create areas of transpression and transtension, oblique contraction is accommodated in the Transverse Ranges, while oblique extension occurs in the Walker Lane fault systems (Figure 11; Dickinson, 1996; Wesnousky, 2005). While the Walker Lane fault
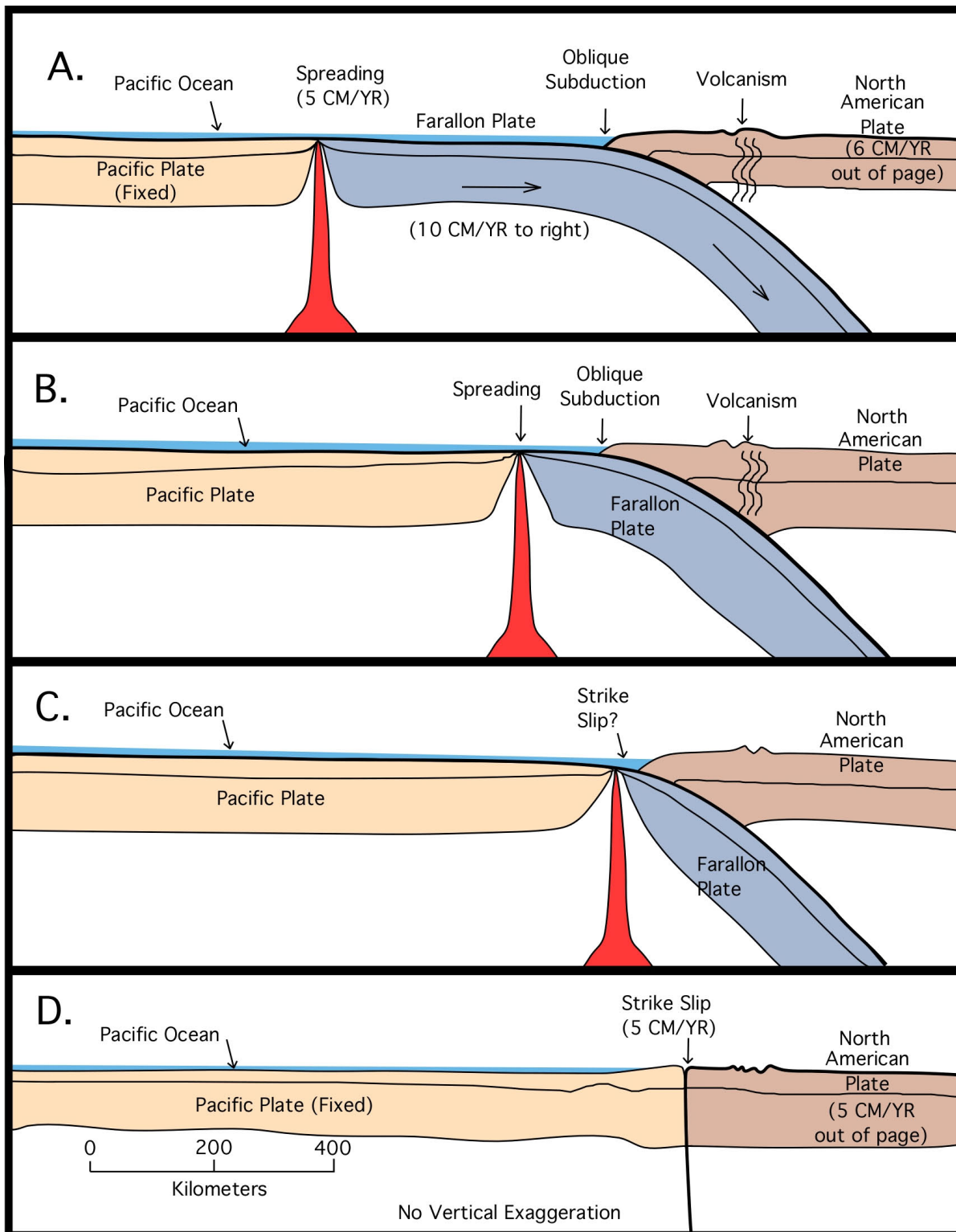
Figure 9. Cartoon of plate-scale cross-sections showing the evolution of collision between a mid-ocean ridge and a trench. As the Farallon plate nears the trench it is still hot, young and easily deformed. *A.* represents the plate configuration in the early Tertiary, *B.* shows the spreading center approaching the trench, *C.* represents situation where ridge and trench collide, *D.* represents present plate configuration. (Modified from Atwater, 1970)
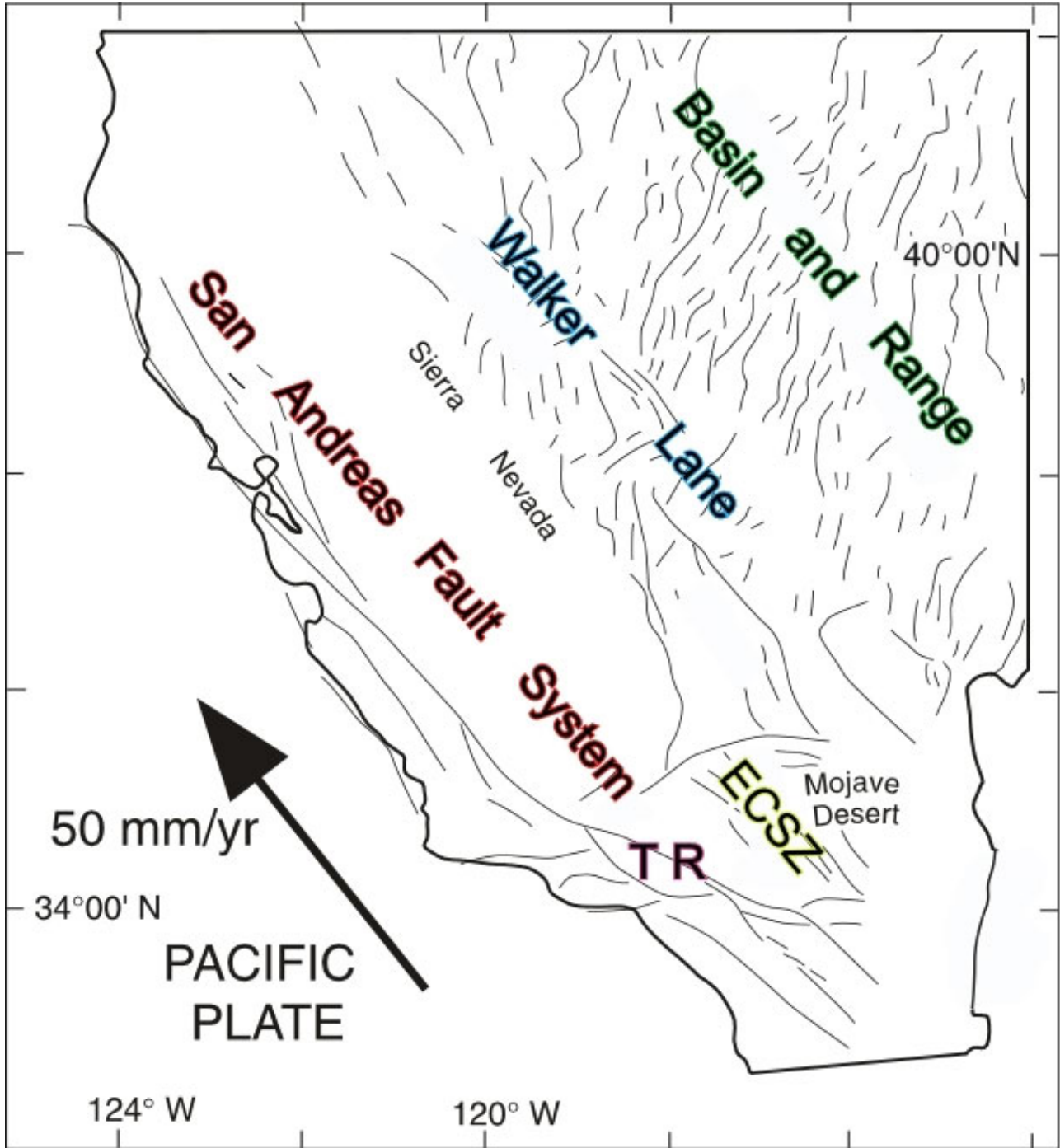
Figure 10. Fault systems that accommodate transform motion between the Pacific – North American plate boundary system. ECSZ = Eastern California shear zone. TR = Transverse Ranges. Modified from Wesnousky (2005).

A.   Oblique Extension
or
Transtension

B.   Oblique Contraction
or
Transpression
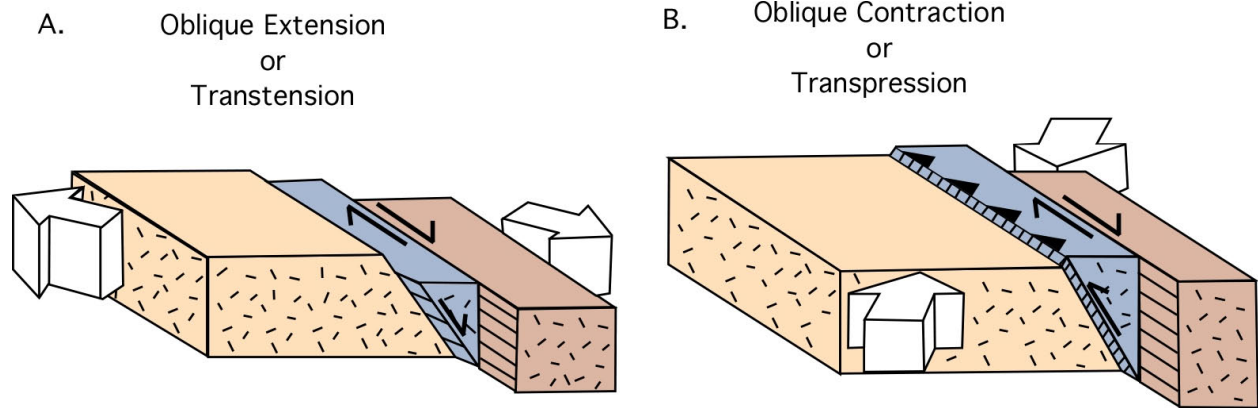
Figure 11. The oblique component of movement along the Walker Lane (A.) and Transverse Ranges (B) create transtensional and transpressional strike-slip systems, respectively (Redrawn from Wesnousky, 2005).

system does take up some of the motion between the North American and Pacific plates, it is estimated that the structurally more mature San Andreas fault system has undergone 3-4 times more lateral displacement than the discontinuous Walker Lane system (Wesnousky, 2005).

2.2 Previous Work on Agua Blanca Fault

Allen *et al*. (1960) conducted the first comprehensive study of the Agua Blanca fault. The authors describe the fault as a major right-lateral strike-slip fault with an unusual trend that is oriented ~30° counterclockwise to the overall orientation of the San Andreas fault system, which otherwise dominates the tectonic grain of the region and has a more northwest-southeast orientation (Figure 1). Allen *et al*. (1960) postulate that this unusual trend resulted in order to accommodate the so-called "great bend" in the San Andreas fault system in southern California west of the Eastern California shear zone (Figure 10), where the San Andreas has a major left-bend creating a zone of transpression (Figure 11). The unusual trend of the Agua Blanca fault may be the result of reactivation. Moore (1969) and Gastil *et al*. (1981) suggest that the Agua Blanca fault originated in the Late Cretaceous and was more recently reactivated in order to accommodate the opening of the Gulf of California.

The Agua Blanca fault can be traced for ~120 km from the Pacific Ocean to almost the Gulf of California. Along the western extent of the fault near the Pacific Ocean, the fault is split into two divergent faults. Here, a more recently active northern section trends in a more northwesterly orientation, while the original southern section (Santo Tomas fault) has more of an east-west trend. These two fault branches apparently join farther to the east in the Valle Santo Tomas (Figure 3). The adjacent valley to the east is the Valle Agua Blanca, which has been designated by Allen *et al*. (1960) as the type locality for the Agua Blanca fault. From here, the

easternmost portion of the fault runs from Valle Agua Blanca to Valle de Trinidad (Figure 3), where it terminates near the Sierra San Pedro Martir escarpment.

In Valle Agua Blanca, the fault is limited to one narrow zone that is in part a structural trough and shows many of the expected features associated with strike-slip faults including scarplets, right-lateral stream offsets, shutter ridges, and sag ponds (Allen *et al.,* 1960; Hatch, 1987). Allen *et al.* (1960) recognized distinctive fan gravels that have been laterally offset from their original location by about 5 km, while some crystalline bedrock shows displacement of up to 23 km. Thus, these authors estimated fault displacements ranging from 5 to 23 km (Allen *et al.,* 1960).

Rockwell *et al.* (1987; 1993) conducted trenching and geomorphic studies in a few widely spaced locations along the Agua Blanca fault and used their observations along with soil chronology to develop slip rate estimates. Radiometric ^{14}C-dating of charcoal and correlation of soils to deposits of known age were used to develop the soil chronosequence. Categorization of Quaternary deposits and quantification of recognizably offset landforms such as deflected stream courses, shutter ridges, and offset canyon walls allowed estimates of displacement rates. If only Quaternary deposits are considered, the slip rate for the Agua Blanca fault has averaged 4 mm/yr over the past 28 ka for the main Agua Blanca fault. In Valle Agua Blanca the slip rate estimates increase to 4-10 mm/yr with an average of about 6 mm/yr.

Rockwell *et al.* (1993) also estimated the average earthquake recurrence along the Agua Blanca fault by using slip rate estimates and apparent segmentation of the fault. Surface ruptures 30-40 km in length typically occur with earthquake magnitudes from 6.8 to 7.0. Displacements along a rupture that would accompany an earthquake of that magnitude usually range from about 0.5 to 1 m. Using these two assumptions and an average slip rate of the Agua Blanca fault of 4-6

mm/yr, an average earthquake recurrence interval from 90-250 years is obtained. An alternative method using radiocarbon-dated offset features shows an earthquake recurrence interval from 100 to 375 years (Rockwell *et al.*, 1993). Rockwell *et al.* (1993) further noted that evidence for surface rupture as recently as 100-300 years ago was encountered during their trenching studies. If this is correct and the recurrence interval along the fault is anywhere between 90 and 375 years, the fault may have had adequate time to accumulate enough strain to produce a moderately large earthquake in the near future (Rockwell *et al.*, 1993).

Dixon *et al.* (2002) used geodetic data collected from 1993 to 1998 to infer active fault slip rates along the Agua Blanca fault. First, in order to obtain present-day slip rates, campaign GPS data were used to estimate slip rates of about 2.5 mm/yr. Since ambiguity in the slip rate estimate remained, Dixon *et al.* (2002) used these GPS data along with fault geometry, rheological layering and earthquake cycle effects to design several numerical models that illustrate the complex motions of the Agua Blanca and San Miguel faults (Figure 3). A three-dimensional visco-elastic model was chosen to best fit all conditions of the two faults. This model implemented a locked elastic upper crust on top of a more viscous, lower layer that deforms plastically and permanently. The model chosen was designed to take into account both the motions of the Agua Blanca fault and the San Miguel fault. Results of this model showed a combined slip rate across the Agua Blanca fault and San Miguel fault from 4.7 to 7.9 mm/yr. If these rates are correct, then these two faults account for 10-15% of the overall motion between the Pacific and North American plates (Dixon *et al.*, 2002). These calculations suggest that the Agua Blanca fault is still active and should not be considered an abandoned fault. In fact, the fault is most likely currently locked and accumulating strain. Seismic hazard calculations have shown that the Agua Blanca fault is capable of an earthquake with a magnitude between 6.1 and

7.0 every few hundred years. Evidence suggests that the last earthquake along the Agua Blanca fault occurred between 1750 and 1875, a minimum of 135 years ago (Rockwell *et al*., 1993). Assuming these calculations are correct, then the Agua Blanca fault is due for a substantial earthquake in the near future.

2.3 Bedrock Geology

The bedrock in the study area is comprised of the Santiago Peak Volcanics. The Santiago Peak Volcanics were formed subaerially in the Early Cretaceous and are the remnants of a continental margin volcanic arc that existed along the continental margin of western North America. Herzig (1991) interprets the formation as the result of initial phases of arc magmatism. Sequences of volcanic material consist of subaerial mass flow deposits of basaltic-andesite, rare basalt, welded tuff, and pyroclastic flow deposits interbedded with tuffs and ignimbrites. Volcaniclastic breccias are the most abundant lithology of the formation (Herzig, 1991).

Chapter 3: Methods and Results

3.1 Field Areas

Preliminary reconnaissance in the Valle Santo Tomas was carried out in order to find an acceptable area for study (Figure 12). In this initial part of the study we searched for an area that included sufficient evidence for faulting and would be a good location for detailed mapping. Certain areas were eliminated due to a combination of factors including poor exposure, lack of evidence for faulting in the area, excessively steep or rough terrain or dense vegetation.

The area that was chosen for study in the Valle Santo Tomas is situated just to the east of the junction where the more southern Santo Tomas fault joins with the main trace of the Agua
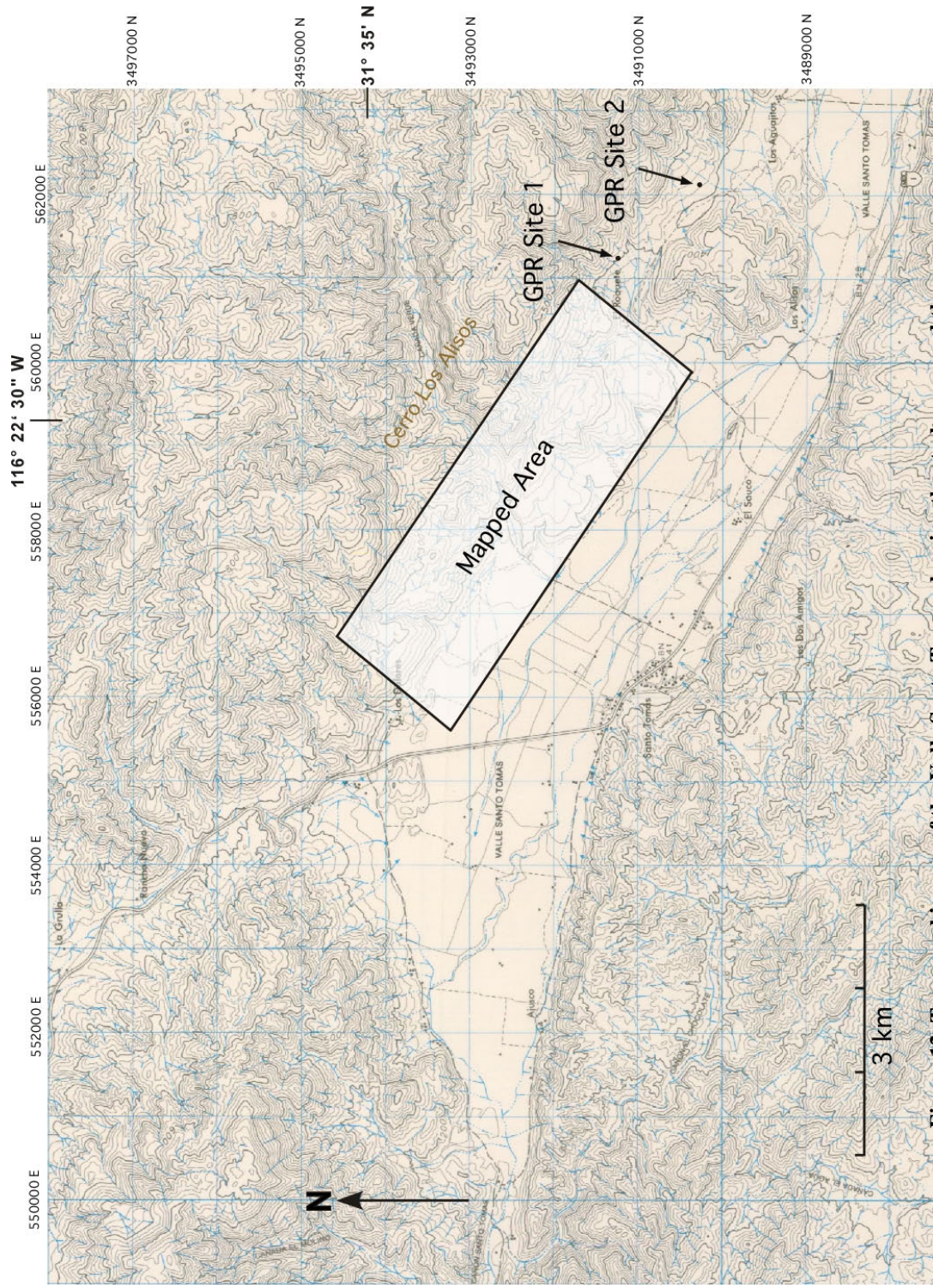
Figure 12. Topographic map of the Valle Santo Tomas showing the study area and the locations of the two GPR surveys. The topographic map is a section of the Rodolfo Sanchez Taboada quadrangle (Quadrangle number H11B22).

27

Blanca fault. The study area lies on the northeast side of Valle Santo Tomas, where the main Agua Blanca fault trace passes along the front edge of a west-northwest-trending mountain range. The mountain range that flanks the basin and the study area to the northeast is named Cerro los Alisos (Figure 12).

After identifying a viable field area for mapping, we determined that the location was still not ideal to conduct a GPR survey. Problems in the field area included either too rugged or steep terrain for the GPR equipment, poor exposure of the fault that did not allow pinpointing its exact location, or heavy and dense vegetation covering the inferred fault trace. For these reasons, a separate site 500 m to the southeast of the map area was chosen for the GPR survey (Figure 13). Another ~500 m to the southeast of the first site a second location was identified and deemed appropriate for a second GPR survey (Figure 13). The geology in this area was mapped by Kretzer (2010) and the second site was shared for GPR surveys using 50 MHz (Kretzer, 2010) and 100 MHz (this study) antennas in order to image the fault in the shallow subsurface.

3.2 Geologic Mapping and Classification of Quaternary Alluvium and Terraces

The area chosen for mapping lies on the northeastern side of the Valle Santo Tomas along the Cerro los Alisos mountain front (Figure 12). The field area is ~5 km long and ~2 km wide for a total of ~10.5 km^2. The rectangular map area is oriented in a northwest-southeast direction with the boundaries aligned roughly parallel and perpendicular to the trend of the fault trace. The geology and geomorphology of the study area were mapped in detail at a scale of 1:5,000 in order to gain a basic understanding of the nature of the geology in general and the fault in particular (Plate 1).
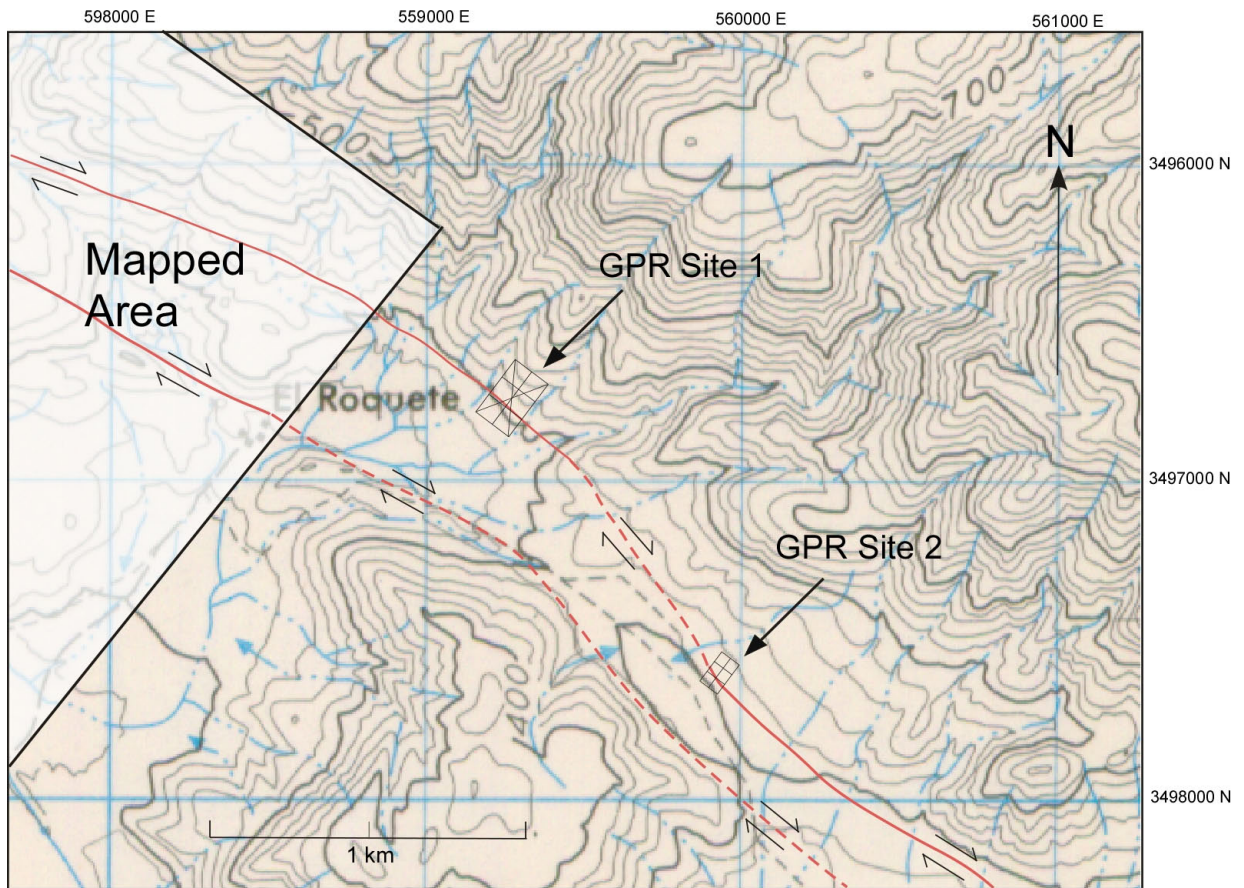
Figure 13. Map showing the location of GPR sites 1 and 2 in relationship to the study area. Fault traces outside of the mapped area are from Kretzer (2010).

To gain an understanding of the nature of the Agua Blanca fault, the exact location of the fault, minor fault splays, and any physiographic features or evidence for recent faulting were identified. The location of the main Agua Blanca fault trace was relatively easy to establish through the identification of scarplets, stream deflections, zones of crushed rock, pressure ridges, sag ponds, and shutter ridges and mapping of local bedrock, alluvial deposits, and structural troughs (Plate 1). The bedrock in the area is exposed at higher elevations in the Cerro los Alisos mountains northeast of the study area and is composed of various volcanic and volcaniclastic units that were not considered in detail as part of this study. Many different lithologies were noted and medium- to dark-grey debris flows with ash to boulder size clasts are abundant in the study area (Figure 14). However, thin alluvial cover on top of the bedrock made it increasingly difficult to determine thicknesses and establish through-going contact relationships between the bedrock units.

The Quaternary alluvial deposits within the study area are apparently derived from the local volcanic bedrock. Generally, the alluvium ranges in size from boulder- to sand-sized particles, but is dominated by fresh, angular gravel and gravelly coarse sand. Quaternary alluvial deposits fill the valley (Valle Santo Tomas) itself, as well as overlie basement rocks in much of the study area along the fault trace. Near the valley floor, sediment is mainly coarse sand with dispersed cobble-sized clasts appearing throughout the deposit. Grain size is generally increasing with higher elevations. Deposits in the study area include fluvial terraces, alluvial fans, and channel deposits.

Figure 14. Photo of unit with large pumice clast within the Santiago Peak Volcanics. Hammer for scale is 30 cm long.

Quaternary units in the study area are divided into seven separate groups (Qa1, Qa1a, Qa2, Qa3, Qa4, Qt1, Qt2) based on inferred age of formation, apparently similar origins, and similarities in morphology and topographic location. Qa1 is the material that is currently transported and deposited in active stream channels. These intermittent streams are reworking, eroding and transporting the older Quaternary sedimentary and Cretaceous volcanic deposits. Most of the stream channels are fairly shallow (~2 m) indicating that they are young or that the streams have recently changed paths. Qa1a in the field area represents the material that makes up the flat-lying valley bottom where the sediments are building the riverbank deposits for the Santo Tomas river, which incises these deposits and transports them towards the Pacific Ocean. The Santo Tomas river itself is an intermittent stream that is currently strongly modified by anthropogenic agricultural practices. Most of Qa1a consists of unconsolidated sand-sized sediments. Qa2 is mainly comprised of loose alluvial materials including sand and cobble size clasts, which make up the active alluvial fans throughout the study area. These alluvial fans are mostly located at the base of the mountain front where small arroyos intersect the main valley floor or form along the more deeply incised canyons such as Canada Verde (Plate 1). Qa3 consists of older alluvial fans throughout the study area containing coarse sand, angular gravel, and boulder sized clasts. These fans are inactive and are currently being eroded and incised by ephemeral streams. Qa4 is comprised of the oldest alluvial fans containing coarser sediments and are topographically higher than Qa3. These alluvial fans are also inactive and currently being eroded. Alluvial fans of the same unit, apart from unit Qa4 that tends to be smaller and more segmented than other units, coalesce with one another and extend for up to two kilometers along the range front in the study area. Individually, fans that are part of units Qa2 and Qa3 are about

several hundred meters in width and retain a convex cross profile and segmented radial profiles (Schug, 1987).

Two different Quaternary terraces (Qt1 and Qt2) are identified in the field area. These terraces are long, relatively level surfaces of unconsolidated material deposited by running water that are bounded on one side by a steeper descending slope and along the other side by a steeper ascending slope (Gary *et al.*, 1974). Qt1 is a lower terrace level, south of the main canyon (Canada Verde) and southeast of Cerro El Roquete (Plate 1). Only a small, ~500-m-long remnant of this terrace remains just above the descending slope of Qa2 and below the ascending slope of Qa3. Qt2 are remnants of a much more extensive, broader terrace that stay at fairly constant elevations from 200-300 m across the field area. This alluvial terrace is cut into bedrock and is covered by a relatively thin veneer of alluvium. The terrace stretches the entire 5 km length of the study area aside from one large break ~500 m wide where it has been incised by Arroyo Verde.

In addition to the main Agua Blanca fault, which is here referred to as the southern trace, another subparallel, subsidiary fault is located just to the north (Plate 1) and appears to be continuous throughout the map area. Both the northern and southern faults are located in linear troughs oriented in the expected direction of the fault trend and both of the faults also show evidence of the physiographic features mentioned above. These troughs, which are probably partially shaped by flowing water, varied substantially in depth and width.

Deflected streams are the most common geomorphic features in the study area. They appear on both fault traces. A series of deflected streams are prominent along the southern fault splay near the northwestern edge of the map area (Plate 1). Each stream channel is nearly identical in width, shape, orientation and length as they erode into the steep mountain face from

northeast to southwest. These channels are ~10 m wide with lengths of ~300 m from the top to the bottom of the mountain face. Near the mapped trace of the fault at the bottom of the slope, these stream channels take a turn to the west before continuing in their down-slope direction where they reach the valley floor and turn to the southeast (Figure 15). It is uncertain whether the final turn to the southeast in this set of gullies is the natural path taken by the streams, or is a result of man-made modification of the streams by agricultural practices.

Another set of five deflected streams is encountered in the northeast corner of the study area along the northern branch of the fault (Plate 1). The three westernmost streams in this set are comparable in width, shape, and length to the first set, but the flow direction is almost due south as they all empty into a small basin (Figure 16). These three streams are deflected ~15 m to the west before continuing downstream and encountering a ridge that diverts the streams to the east. The other two deflected streams farther to the east also flow nearly directly south, but travel down a steeper incline. As they approach the fault, there is a deflection of ~20 m to the west across the fault before the streams continue in the downhill direction for ~5 m. At that point, they encounter a ridge that diverts the streams almost 90° to the east (Figure 17).

Six ridges of varying sizes are encountered throughout the mapped area (Plate 1). Four of the five are found along the northern fault trace and all ridges are located on the southern side of their respective fault traces. These relationships are expected because streams are flowing downhill from the higher elevations associated with the Cerro los Alisos mountains to the north. The first of these features, starting from west to east, is found at the western edge of the study area along northern branch of the fault (Plate 1). This large ridge diverts several streams to the west before the streams are able to exit the canyon. The next ridge to the east along the northern

Figure 15. Picture taken of westernmost deflected stream in the set of six near the northwestern edge of the field area. Blue line shows stream being deflected to the west before reaching the valley bottom and turning to the southeast. View is to the southwest.

Figure 16. Picture of southern and northern faults, ridges, and deflected stream just to the northwest of El Roquete Ranch. Area encircled in yellow and red outline the ridges; blue line shows deflected stream; solid black line is the southern fault; dashed line is the northern fault. Insert shows location and map view of the picture. Dot with arrow on the insert shows the location and direction from where the picture was taken.

Figure 17. Solid blue line shows two streams joining before being deflected to the right (west) near the fault before turning back to the east. Dashed blue line shows location of the stream after it travels behind a ridge. Area encircled in yellow is a ridge that causes the stream to turn to the east. Fault runs directly in front of ridge along dashed blue line. Picture taken towards the southeast above the northern branch of the fault just to the north of El Roquete ranch.

branch of the fault closely resembles the previous. This feature is at the same elevation and lies along the same mountain face as the first ridge. However, the streams are diverted to the east, rather than the west in order to flow around the obstacle. The following ridge to the east is a large feature composed of Cretaceous volcanics named Cerro el Roquete. Cerro el Roquete is the largest of the noted ridges reaching an elevation of 280 m and blocks a canyon to the north, which causes multiple streams to be diverted to the northwest. The next ridge lies at the far eastern side of the study area and is the only one to lie on the southern branch of the fault. In this case, multiple streams are blocked and have been forced to flow to the east to go around the impediment before turning to the southwest (Figure 16). The fifth ridge is located in the northeastern corner of the study area along the northern branch of the fault. This ridge causes a near 90˚ change in direction of flow of a deflected stream from the south to the east over a distance of a few meters (Figure 17). A sixth ridge is located just to the west of El Roquete ranch north of the southern fault (Plate 1). This ridge is ~100 m long and ~20 m wide with a height of ~4 m in the center.

A small pond forms along the southern branch of the fault in the central part of the study area just to the west of Cerro El Roquete (Plate 1). Water was not present in the depression, but a sag in the rock and sediment is clearly evident in the area. The depression is fairly circular in shape with a diameter of ~50 m.

A 15-20 m high scarplet on the northern fault is present ~250 m to the northwest of the pond (Plate 1 and Figure 18). Here, on the south side of the fault, sediment fails and slides down a steep slope as the area of the fault trace is eroding away creating an oversteepened slope. A pile of sediment at the bottom of the slope and relatively fresh soil along the scarplet surface makes the landform easily identifiable (Figure 18).

3.3 GPR Sections and Descriptions

3.3.1 GPR Survey Locations and Transect Processing

GPR survey sites 1 and 2 were chosen because they were accessible with GPR equipment, moderately sloped, and located across an apparent fault scarp (Figure 19). Identifying the fault trace was essential in order to be certain the survey was taken across the fault.

The GPR system utilized for fieldwork is a pulseEKKO® 100 made by Sensors and Software Incorporated. The control unit along with the Digital Video Logger (DVL) are attached to a backpack for ease of transportation to survey areas and during data collection. A grid arrangement of transects was chosen for the design of the GPR surveys (Figure 20). The design for both sites was chosen to maximize continuity of the transects and ultimately attempt to show the subsurface in three dimensions. A set of transects intersecting the fault at a perpendicular angle is tied together with transects running parallel to the fault as well as two diagonals in order to maximize the linkage of subsurface features and elevations of the surface. Extensive brush was cleared along the transect lines in order to have the best possible contact between the antennas and the ground and to ease transportation of the cumbersome antennas along the lines. The grids were constructed using measuring tape, wooden stakes, and string. Stakes were placed in the ground every 25 m to attach string and insure the transect lines were strait.

Figure 18. Picture of fault scarplet on the northern fault looking to the southeast. Dashed, black line shows the location of the fault trace. Thin, solid black line outlines the scarplet. Fault is right-lateral.
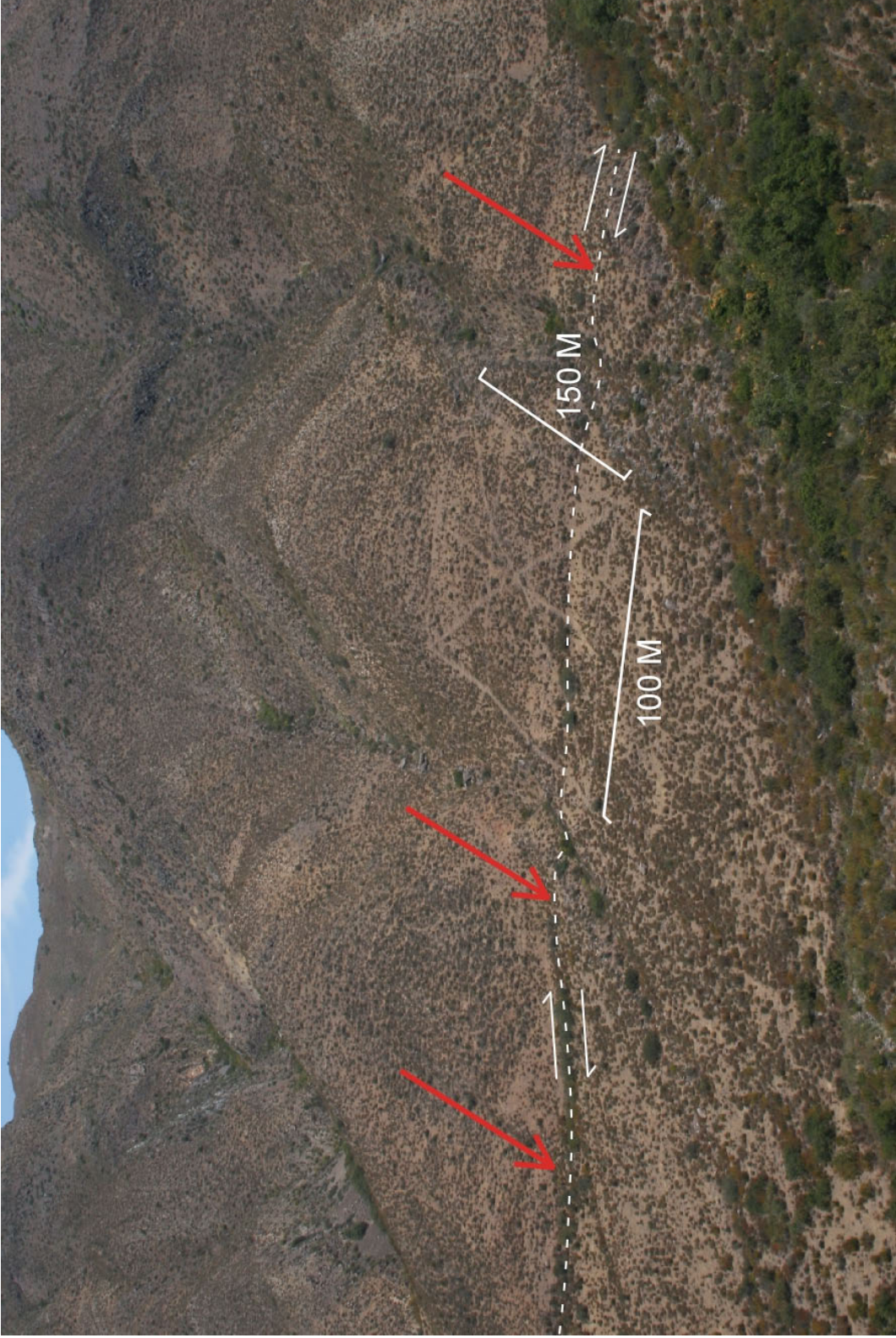
Figure 19. Location of GPR Site 1 viewed towards the north. Red arrows point to the fault scarp; White dashed line follows the fault trace. GPR grid is visible by the cleared vegetation. Long side is 150 m long for scale.

The grid survey points were recorded by taking points every 25 m on each transect with a Trimble GeoXH 2008 GPS System. Traces were continually monitored on the DVL throughout the sampling process. Reflection surveys were used at both sites and data were collected one line at a time on the DVL for each transect.

The 50 MHz antennas were chosen for use at site 1 (Figure 13 and 19). These antennae offer deeper penetration with the best trade off with signal resolution. The grid was 150 m long by 100 m wide with the fault trace intersecting perpendicular to the length (Figure 20). Three 150 m long transects were taken perpendicular to the fault, while four 100 m transects were taken parallel to it. Two diagonals across the grid were completed to help correlate between traces throughout the site (Figure 20). Using a 50 cm step size, all nine reflection surveys (transects) were taken along with a CMP survey in the area to establish the optimum propagation velocity to calibrate the unit. The top 100 m of the grid was placed on top of an alluvial fan before intersecting the fault scarp and continuing below on a lower, more level alluvial fan (Figure 19).

Site 2 is located 500 m to the east of site 1 and overlapped the GPR grid survey site of Kretzer (2010; Figure 13). The 100 MHz antennae were chosen for use at site 2 (Figure 21). The results of these surveys where then used to compare images to data obtained by Kretzer (2010), who used the 50 MHz antennas in the same area. The comparison allows evaluation of the trade off between resolution and depth penetration. The grid design was 75 m long by 50 m wide with the fault trace intersecting perpendicular to the length. Three 75 m long transects were taken perpendicular to the fault while four 50 m transects were taken parallel to it (Figure 20). A step
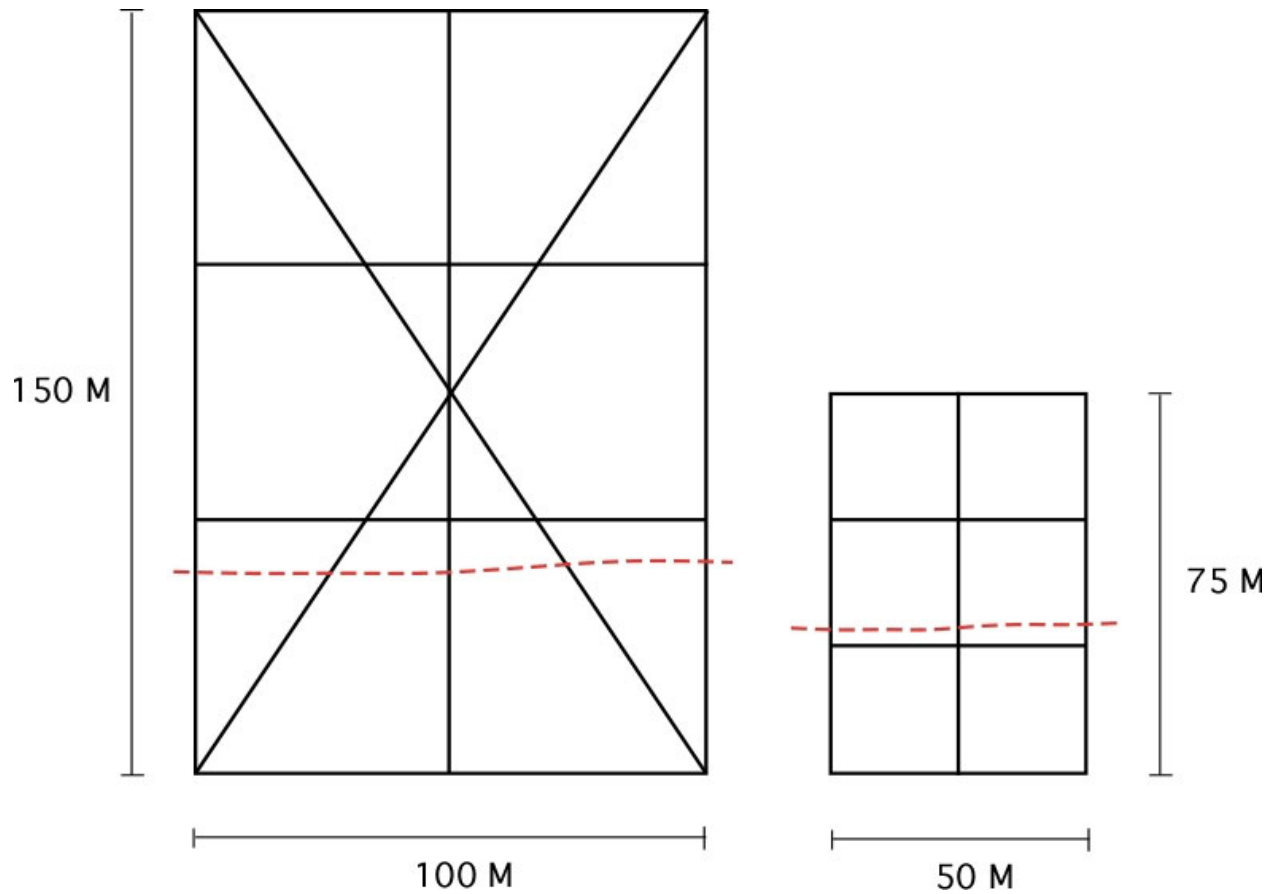
Figure 20. Layout of macrogrid transects for site 1 (left) and site 2 (right). 50 MHz antennas were used for site one and 100 MHz antennas were used for site 2. Red dashed line shows approximate location of fault scarp.

Figure 21. Location of GPR Site 2 viewed towards the south. Red arrows point to the fault scarp; white dashed line shows the fault trace; black lines show the outline of the GPR grid. The grid of Kretzer (2010) is visible in the vegetation. Van for scale on right side (west) of the picture.

size of 25 cm was used for all seven transects at site 2. The top half of the grid at site 2 was laid out on an alluvial fan before intersecting the fault trace and continuing below (Figure 21).

Data stored on the DVL were then imported to a laptop where EKKO_View Deluxe processing and viewing software displays the data collected in the field. The software displays traces taken from every step and aligns them adjacent to one another. This reveals reflections from the subsurface representing different strata. These data are then post-processed to reduce "noise", so that a clearer image emerges that can later be more accurately interpreted. The GPR data are filtered for "wow", or what is known as "dewowing". This process removes a false low frequency signal that is superimposed on the high frequency reflections, which are preserved (Figure 22). After this step, gains may be applied to the data. This processing tool amplifies some of the weaker signals that are recorded in order to compensate for the attenuation of energy. This step helps accentuate changes in strata where there is a minimal difference from one medium to the next, or deeper strata that have weaker returning signals (Figure 23). Any erroneous traces are removed at this point and, if there is a break in data, transects can be reconnected. Next, GPS data including longitude, latitude, and elevations to correct for topography are applied to each transect (Figure 24). The CMP survey conducted in the field is then used to conduct a velocity analysis, where two-way travel time is converted into depth. Finally, a color scheme is applied to the sections to better emphasize subtleties of the nature of the strata in the subsurface and aid in interpretation (Figure 25). The 100 MHz antennas at site 2 produced unwanted noise that could not be deciphered or be used to aid in interpretation of the lines. This spurious noise was subsequently removed only from transects at site 2 (Figure 26). After these steps are completed, the GPR sections are ready for interpretation.
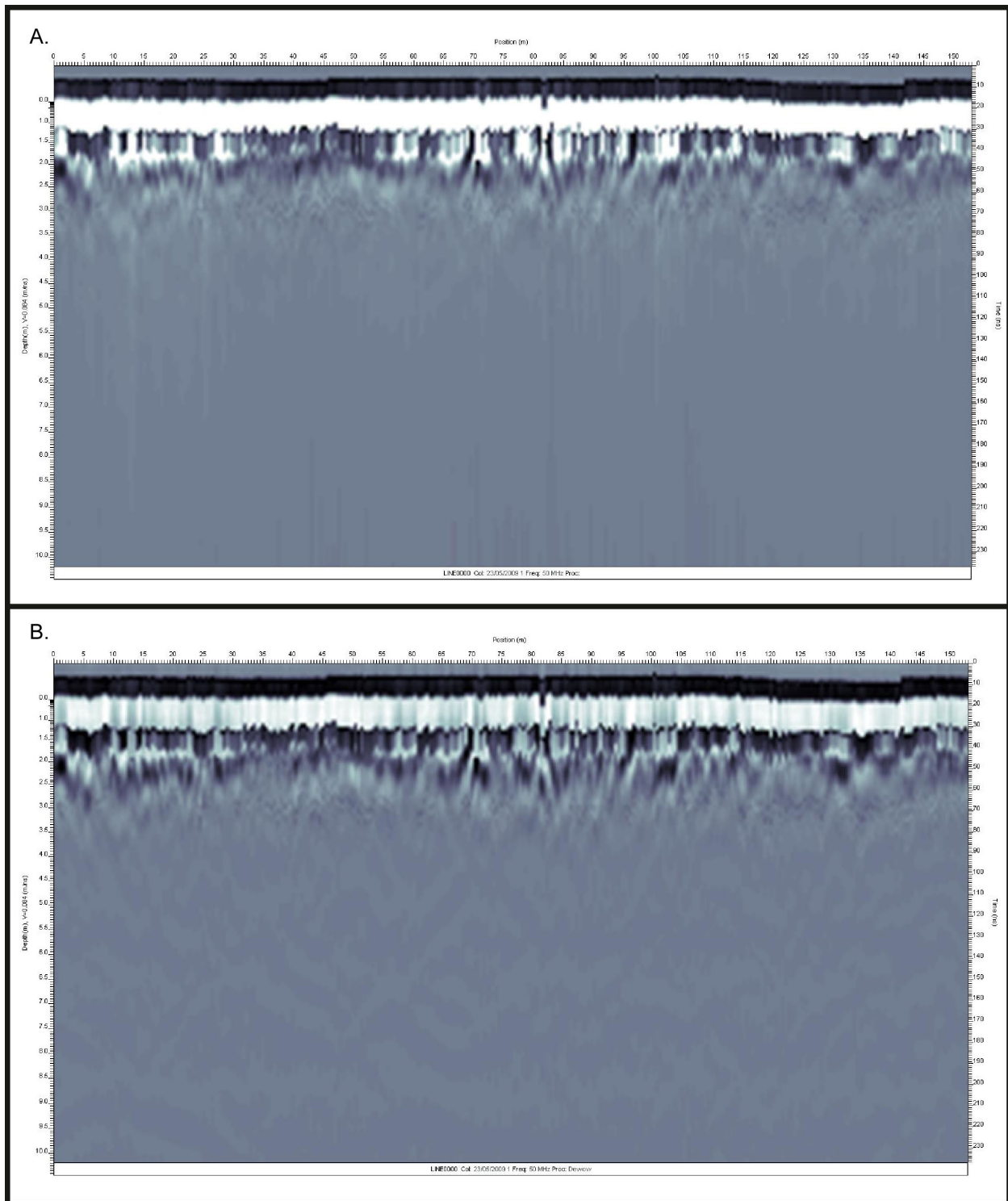
Figure 22. GPR Transect profile from site 1 shown as raw data (A) and after being processed with a dewow filter (B). This process removes unwanted low frequency signals while preserving the high frequency signal.
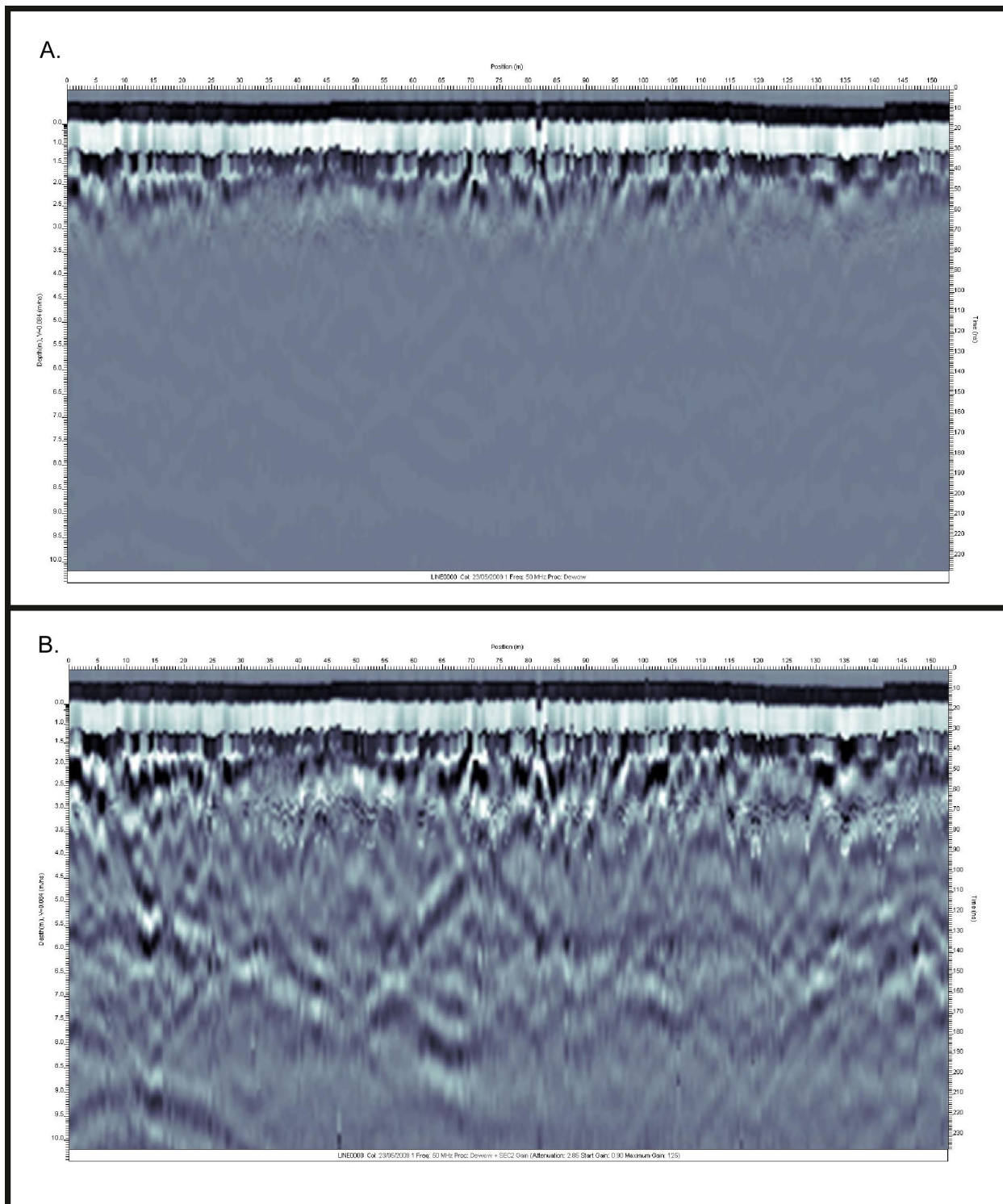
Figure 23. GPR transect profile before (A) and after (B) gains are applied. Gains use the average decay curve of radar signal strength to calculate an appropriate gain function for the dataset.
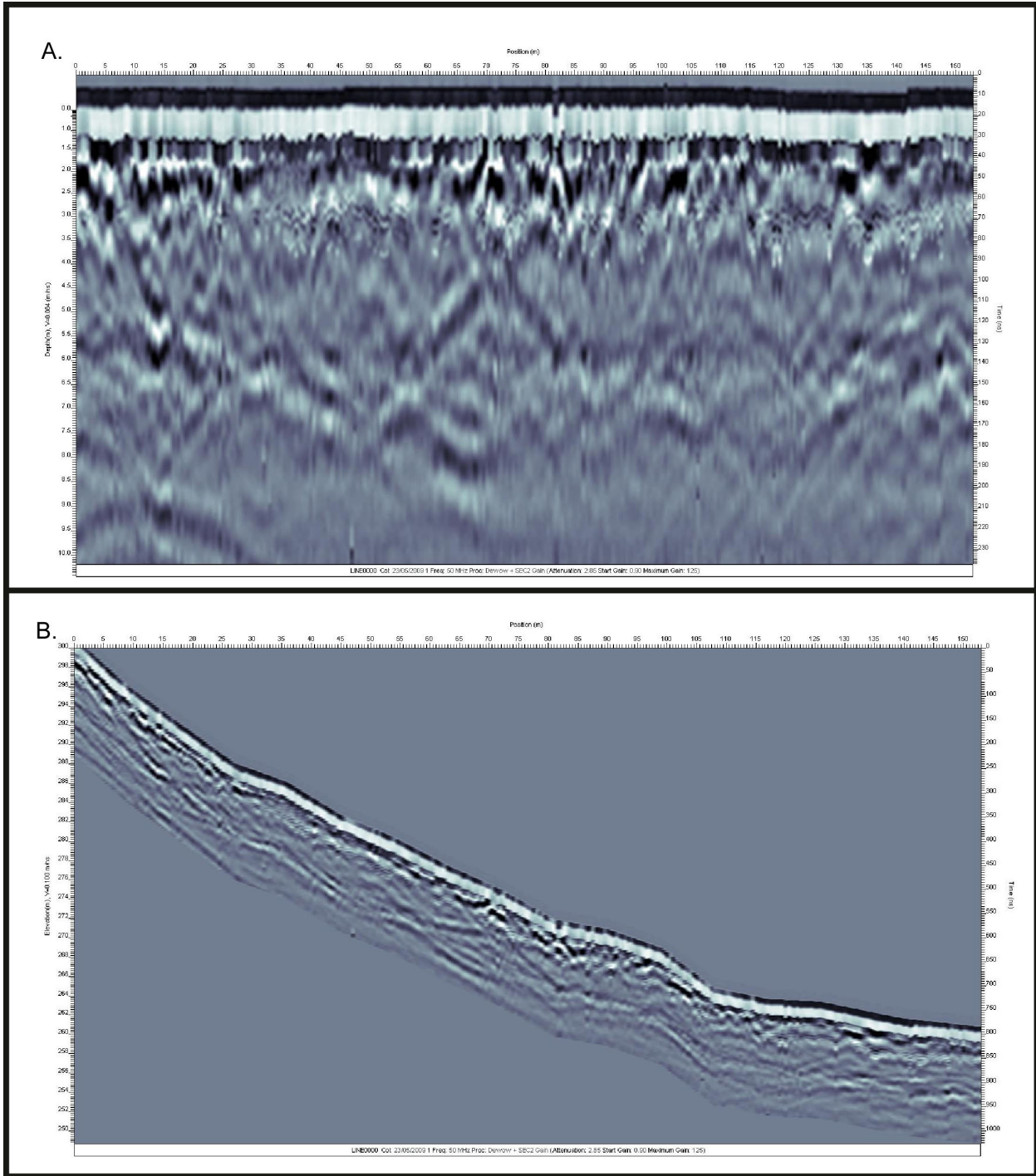
Figure 24. GPR transect profile shown before (A) and after (B) GPS elevation correction.
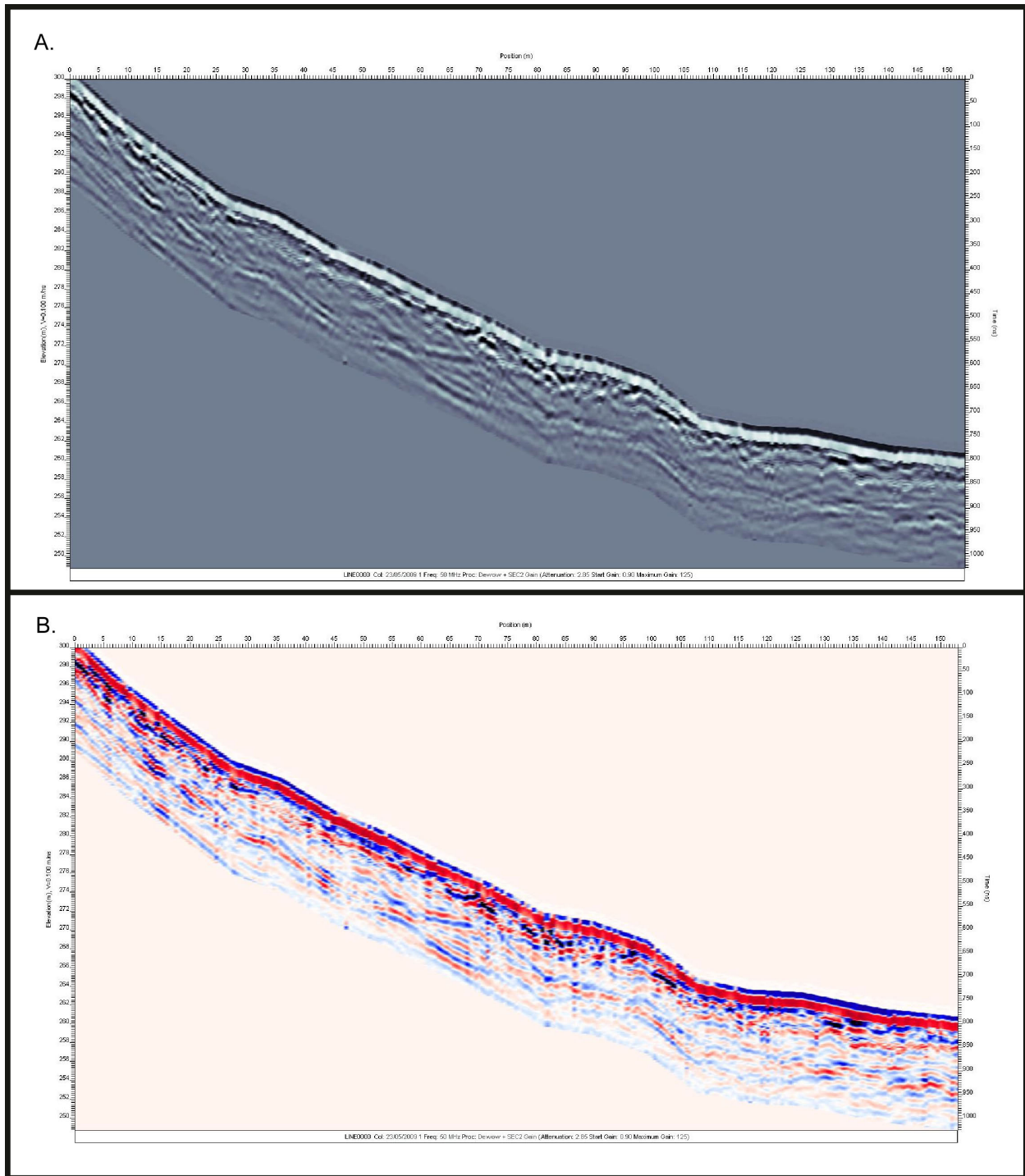
Figure 25. GPR transect profile before (A) and after (B) a color scheme was added in order to accentuate the subsurface nature of the strata.
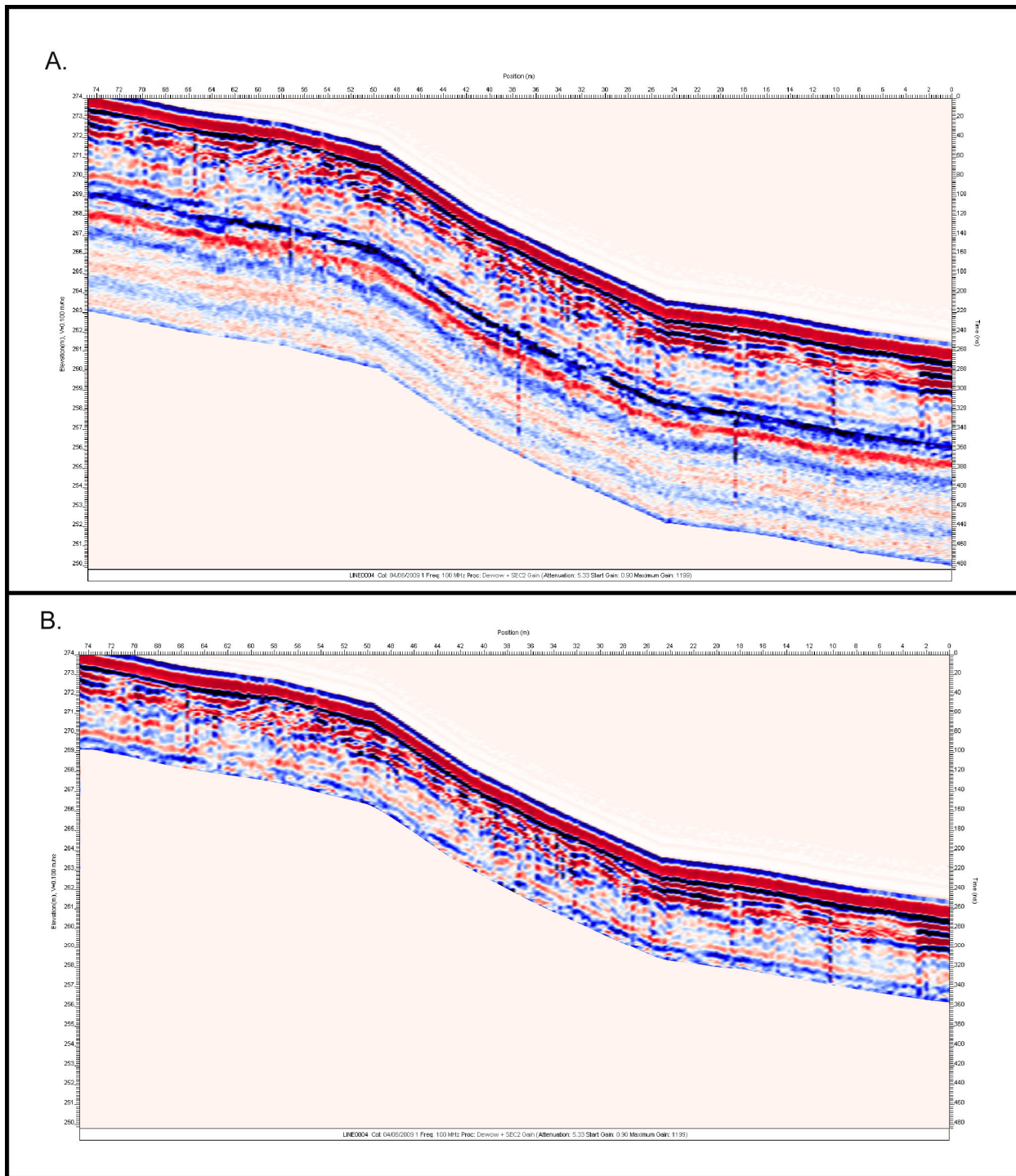
Figure 26. GPR transect profile from site 2 before (A) and after (B) residual noise was removed from the line.

3.3.2 Descriptions of GPR Transects

At each of the sites, the first two signal returns are disregarded as they represent reflections from both the air and ground before entering the subsurface. GPR transects show laterally continuous reflections as well as discontinuous or wavy reflections, convex reflections, and some chaotic reflections. The key feature here is that all transects perpendicular to the fault show the truncation and displacement of continuous lateral reflectors that represent alluvial deposits. The faults in the GPR transects are recognized by laterally continuous signals being truncated and vertically offset along a single, near-vertical plane.

Chapter 4: Interpretations

4.1 Interpretation of Quaternary Alluvium and Cretaceous Volcanics

During the field mapping Quaternary deposits were divided into Quaternary alluvial and fluvial units (Qa1 through 4) and Quaternary terrace deposits (units Qt 1 and 2). Qa units 1 through 4 were based on the relative depositional age with Qa1 interpreted as being the youngest while Qa4 is interpreted as being the oldest. The relative ages tend to correspond to some degree to topography with the oldest units (Qa4) being at the highest elevations along the mountainsides directly overlying Cretaceous volcanics and youngest (Qa1) currently incising and eroding older units and accumulating in Santo Tomas valley. The older Quaternary alluvial units were sites of deposition likely until base level was lowered. Lowering base level can cause deposition to cease entirely along an alluvial fan and begin erosion. Erosion of the older unit should result in formation of and deposition on another, younger fan unit below. Unit Qa4 is interpreted as the oldest alluvial fans deposited along the mountain front and may have been much more extensive in the past, but erosion has since reduced their size. It is likely that the valley floor was much

higher during the formation of Qa4 and that sediment was trapped in the basin during a period where the outflow out of the valley was much more restricted. Evidence for this interpretation comes from the presence of bedrock terraces (Qt2), which could have only formed when the valley was filled with flat-lying sediments to a point where bedrock north of the main fault trace was eroded and formed a level surface. A significant base level change probably occurred when the Santo Tomas river was established and reached the ocean along the trace of the Santo Tomas fault. This caused increased erosion and enabled significant amounts of sediment to exit the valley. A short period of stabilization and lessened erosion resulted in the formation of the lower terrace (Qt1) and the initial formation of the alluvial fans that make up Qa3. Most of Qt1 has since been eroded away. This second adjustment to an apparently shifting base level in Valle Santo Tomas could be related to rapid sea level fall, which caused the valley to erode rapidly once again. At this point, Qa3 continued to form as portions of Qt2 were incised. Qa2 is currently forming along the base of the slope and is generally bounded by Qa3 above and Qa1 below. Qa1 are the flat-lying fluvial sediments deposited along the valley floor, while Qa1a deposits are the currently active eroding streams that incise other units and transport sediment throughout the field area.

In addition to Quaternary units, Cretaceous volcanics (Kv) were identified as the bedrock in the field area (Plate 1). The scope of the study did not include an in-depth analysis of the bedrock in the area and all Cretaceous volcanics were mapped as a single unit. The bedrock is most likely comprised of the Santiago Peak Volcanics. The Cretaceous volcanics in the study area are mostly covered by a thin layer of alluvium throughout the entire field area derived from the formation itself.

4.2 Interpretation of Geomorphic Features

Numerous geomorphologic features commonly associated with faulting are found in the study area. These features include deflected streams, shutter ridges, pressure ridges, scarplets and a sag pond. Probably the most prevalent features in the area are deflected streams. All of them are deflected to the right (northwest) approximately the same distance (~20 m) along the trace of the fault as would be expected in a right-lateral strike-slip fault. However, the stream deflections in the study area are not at 90° angles that would be expected across a very recently active fault with significant displacement. Rather, these streams approach the location of the fault trace and bend approximately 40°-60° to the northwest before continuing along their downhill path (see figures 15, 16, and 17). These bends can be explained, if one considers the likely earthquake recurrence interval (100 to 375 years; Rockwell *et al*., 1993) and maximum displacement during an earthquake (0.5 to 1 m; Rockwell *et al*., 1993). The relatively small amount of displacement may allow enough time for these ephemeral streams to reestablish themselves. Furthermore, the unconsolidated sands and gravels present in the study area, especially along a main range front are very vulnerable to any type of surface erosion by water and can be worn away with relative ease. Lastly, the steep mountain front in the study area results in steep stream gradients where topography can change as much as 160 m in less than half a kilometer. This means streams traveling down this steep slope intersect the fault at 90° and have a great amount of eroding power, causing it to quickly round off any sharp turns that might have been present along the stream. All of these factors combined result in the moderate turns in the offset of deflected streams present throughout the study area.

Ridges that have bee noted previously are interpreted as shutter ridges (outlined in yellow in figures 16 and 17) that have been translated long the fault and shut off canyons that lie to the

north, diverting streams both to the northwest and to the southeast around the impediment. One ridge is interpreted as a pressure ridge and is located just to the west of El Roquete (Figure 16). This ridge is different than others in that it lies at the bottom of a canyon and is smaller than other noted ridges. Here, a slight bend in the fault to the left (south) creates a restraining bend and causes oblique compression in the area. This pressure ridge (outlined in red in Figure 16) forms as a result of one fault block converging with the other at an oblique angle, creating pressure between the two that results in the formation of the ridge. A bend to the right along the fault in another area (Plate 1) creates the opposite affect creating a small depression where oblique extension is taking place in the releasing bend. This depression is interpreted as a sag pond.

Geomorphic features characteristic of faulting have a finite life expectancy. These physiographic features are generally small, erodible landforms whose preservation potential is highly dependent on climate (Sylvester, 1988). Although rainfall is limited in the desert environment of Baja California, the unconsolidated nature of the sands and gravels, lack of protective vegetation, and high relief of the area surrounding the fault suggests that flowing water, when present, is a highly erosive force. These combined factors equate to a short life expectancy of features characteristic of faulting. Thus, the presence of these geomorphic features in the study area indicates rather recent formation, possibly within the past few hundred years.

4.3 Interpretation of GPR Site 1

The GPR grid location was chosen because of the presence of a major fault scarp, which ensured that the fault would be present in the grid area. The 50 MHz antennas at site 1 achieved a depth penetration of ~11 m and produced several quality images with fault splays clearly evident in all

GPR transect lines that crossed the fault at a perpendicular angle (Figures 28-36). Fault planes are interpreted as vertical displacements of reflectors aligned along a plane that intersected at or near right angles to the surface. After completing and analyzing the data, it is evident that offset stratigraphic layers are abundant, which suggests that numerous fault splays are present in the area and that the actual fault scarp probably simply represents the main fault zone. This was not surprising as a study using GPR by Madsen (2009) encountered numerous faults that are not visible at the surface along the Agua Blanca fault. Features interpreted as faults are numerous in transects and range from eight to twelve identifiable fault splays with associated truncations of subsurface strata. Most of these surfaces either reach or come very close to the surface. Faults that do not reach the surface are interpreted as older ruptures that have been covered by fresh alluvium that has not been disturbed by subsequent motion. This motion was probably transferred to surrounding faults in the area. All faults identified are found within 40 m of the scarp located ~50 m above the lowest elevation in the transects.

Interestingly, a large slump that is not apparent in the topography, is seen in all images throughout the upper part of the grid area. This slump is identified by truncations of reflectors by a low angle plane (relative to the surface) rather than the high angle planes that identify faults. The plane of offset reflectors appears at an oblique angle in the subsurface, becomes curved in nature and travels horizontally along a reflector along the lower boundary ~5 m deep. The frontal, or most downhill extent of the slump is recognized through truncated reflectors that are at a slightly higher angle relative to the surface. However, as this plane curves and becomes parallel to reflectors along the lower boundary, it is much harder to recognize. Here, the plane does not travel perfectly parallel to reflectors, but moves up and down creating a discontinuous reflector that signifies the lower boundary (Figures 27-36). The upper boundary of the slump
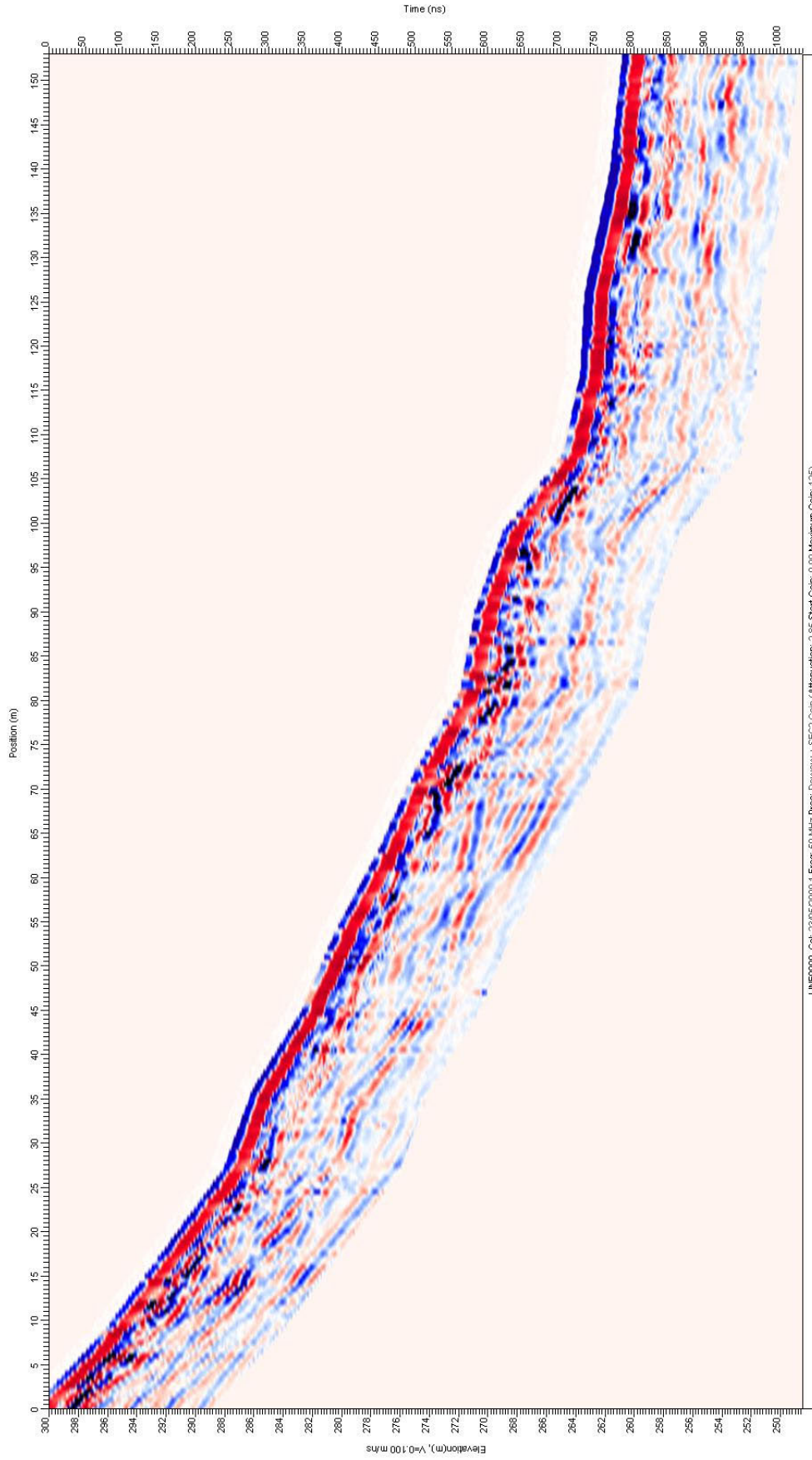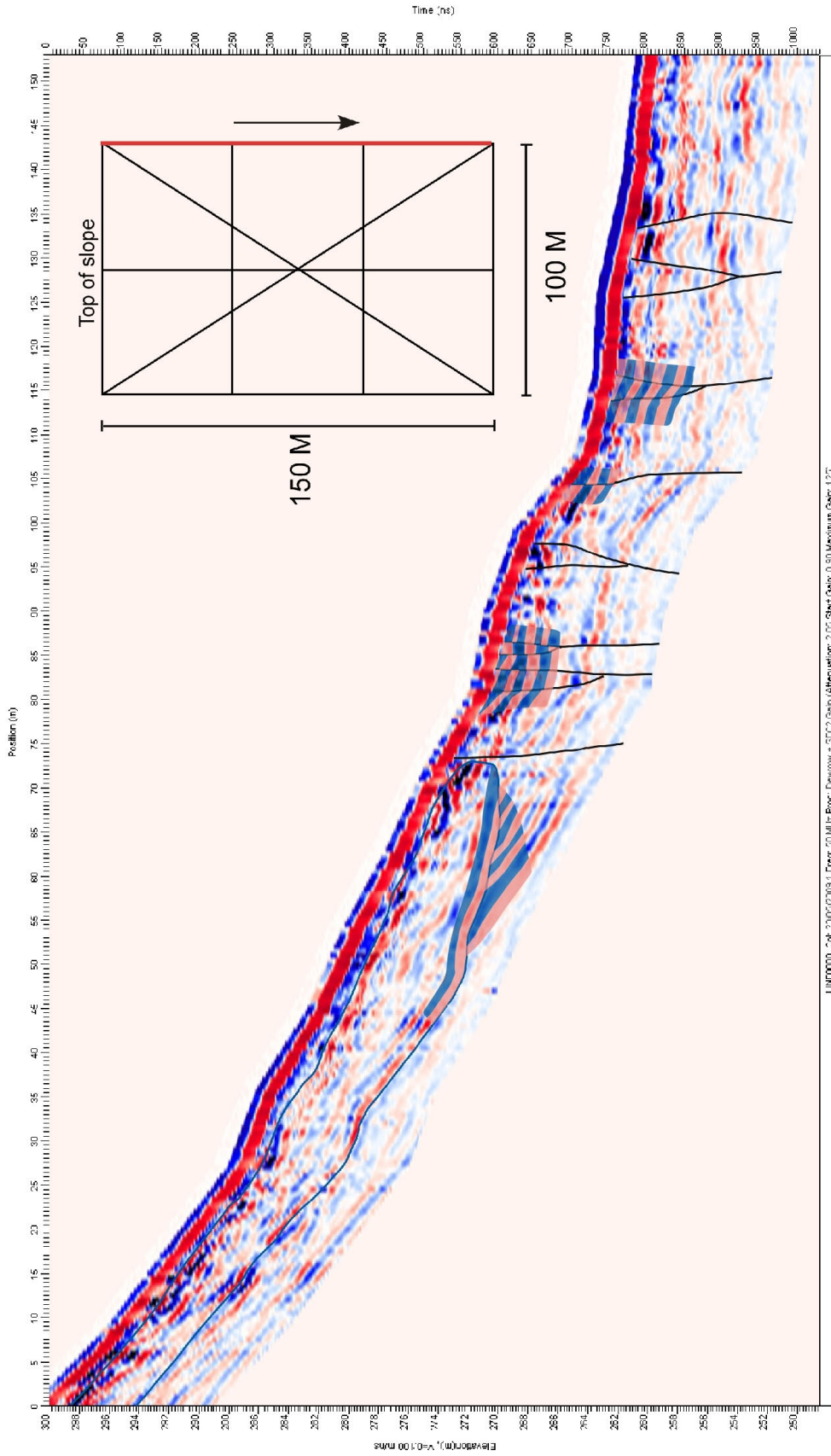
Figure 27. Site 1, 50 MHz, transect 0000 before interpretation.

LINE0000 Col: 23/05/2009 1 Freq: 50 MHz Proc: Dewow + SEC2 Gain (Attenuation: 2.85 Start Gain: 0.90 Maximum Gain: 125)

Figure 28. Site 1, 50 MHz, transect 0000 after interpretation. Black lines represent faults and the dark blue line shows a large slump. Red line on grid shows transect location.

Figure 29. Site 1, 50 MHz, transect 0001 before interpretation.

Figure 30. Site 1, 50 MHz, transect 0001 after interpretation. Black lines represent faults and the dark blue line shows a large slump. Red line on grid shows transect location.
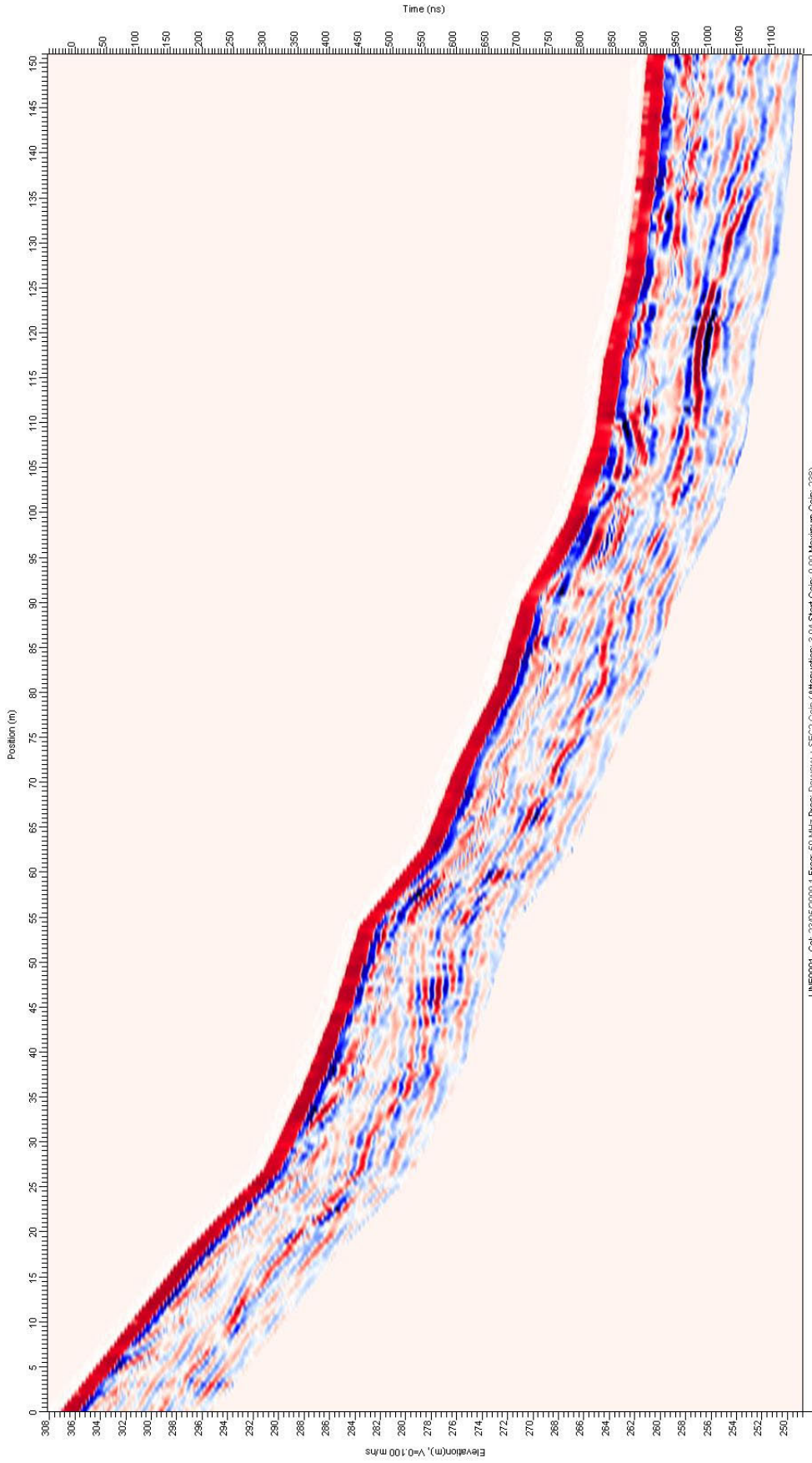
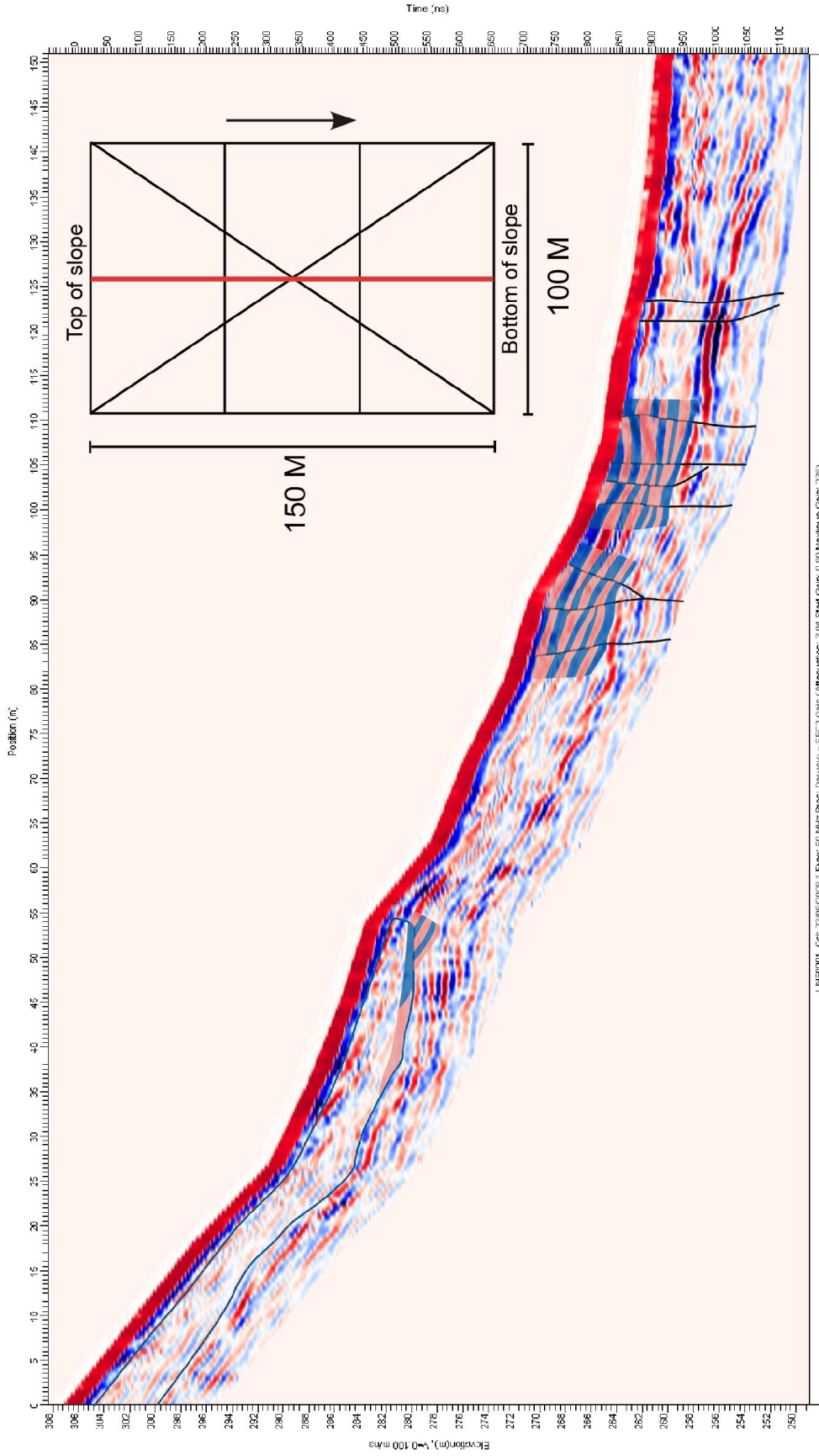**Figure 31. Site 1, 50 MHz, transect 0002 before interpretation.**

Figure 32. Site 1, 50 MHz, transect 0002 after interpretation. Black lines represent faults and the dark blue line shows a large slump. Red line on grid shows transect location.

61
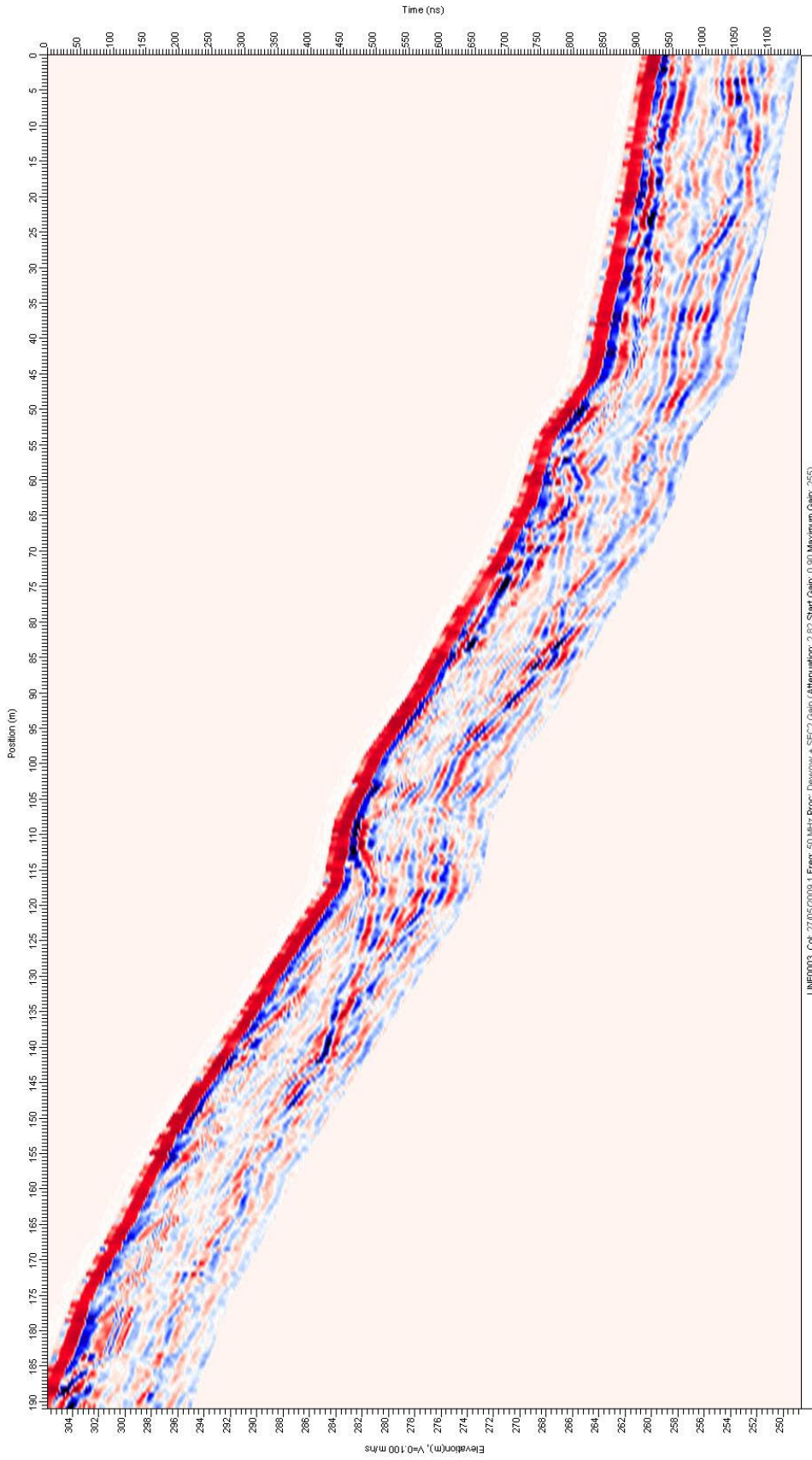
Figure 33. Site 1, 50 MHz, transect 0003 before interpretation.

62

Figure 34. Site 1, 50 MHz, transect 0003 after interpretation. Black lines represent faults and the dark blue line shows a large slump. Red line on grid shows transect location.
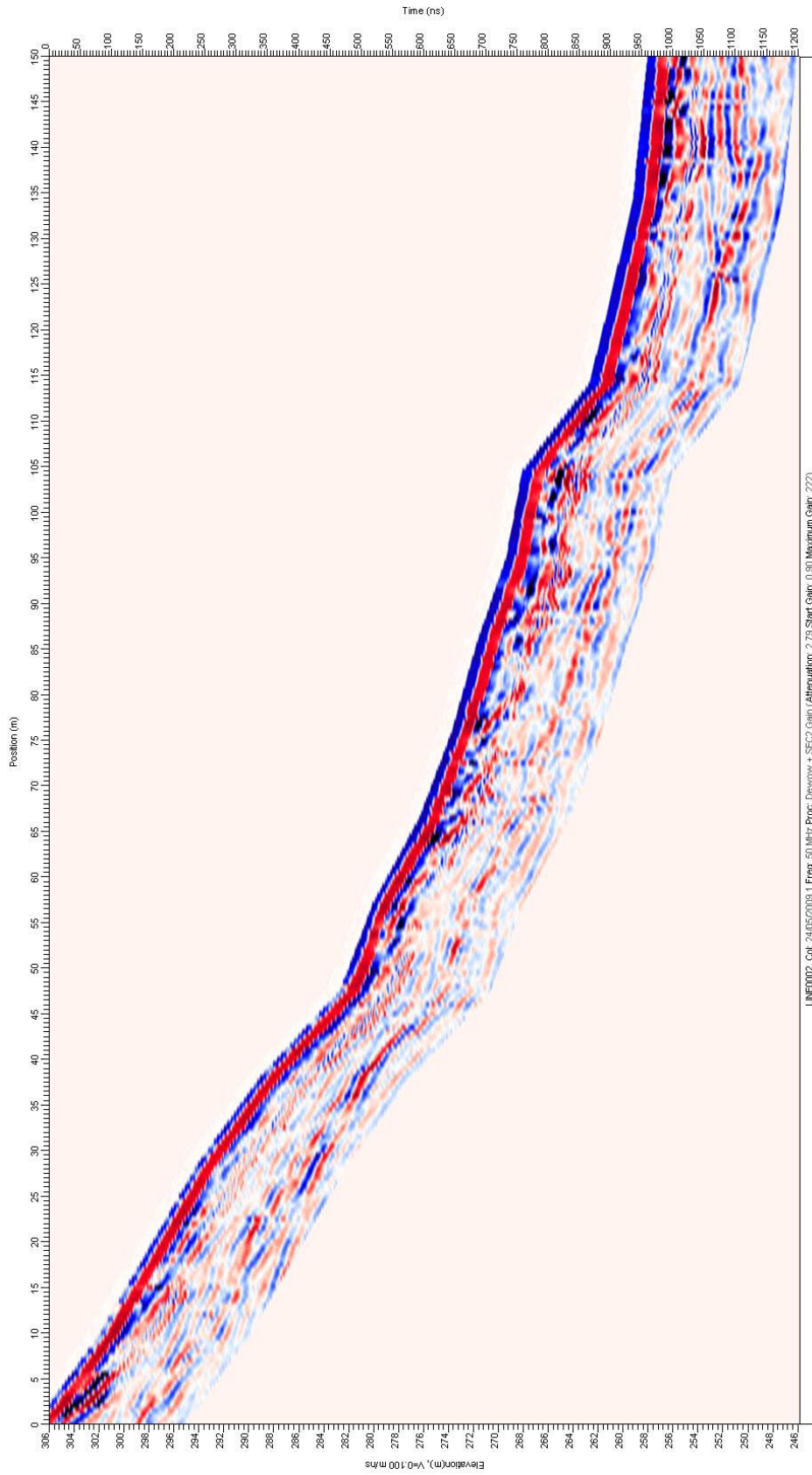
63
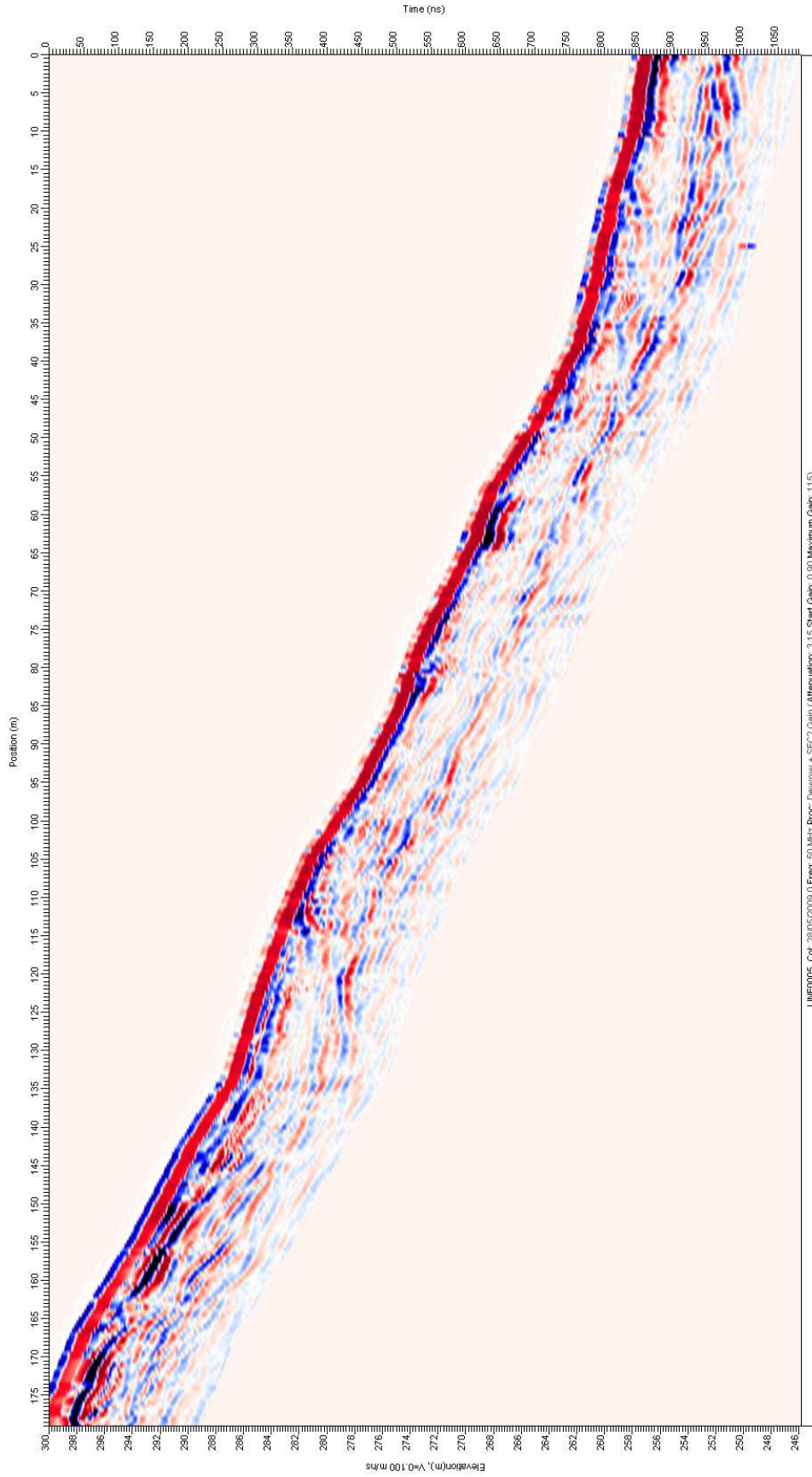
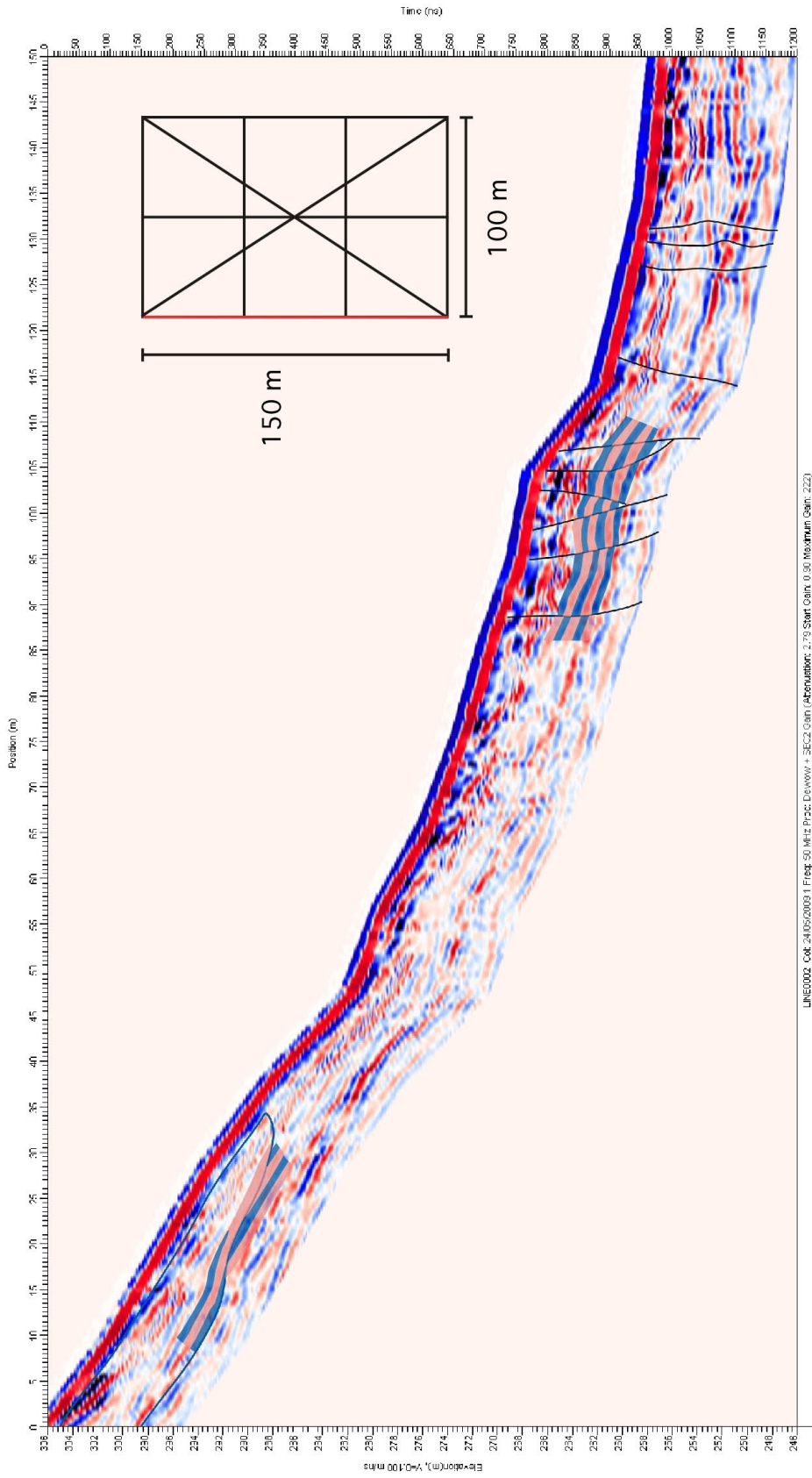**Figure 35. Site 1, 50 MHz, transect 0005 before interpretation.**
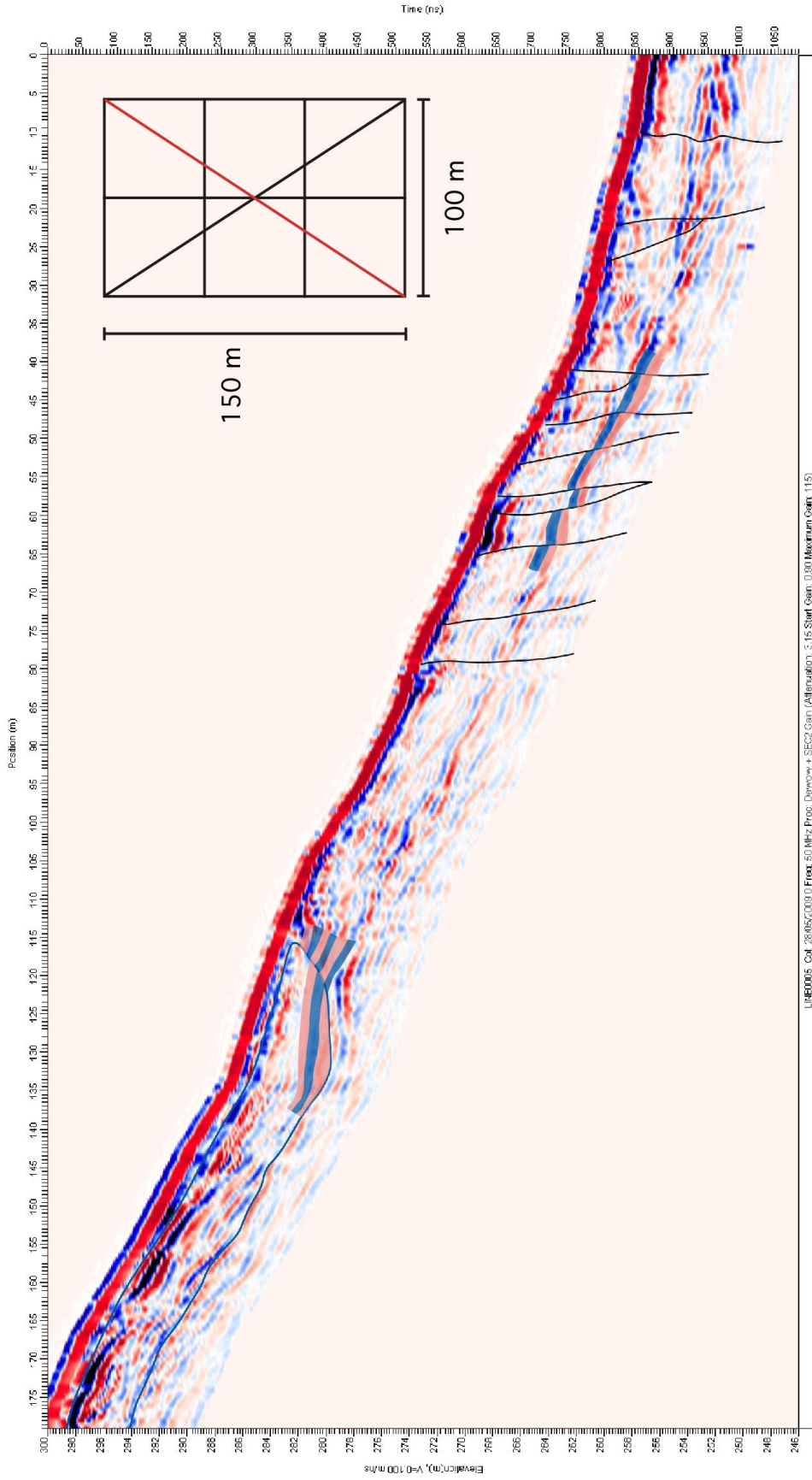
Figure 36. Site 1, 50 MHz, transect 0005 after interpretation. Black lines represent faults and the dark blue line shows a large slump. Red line on grid shows transect location.
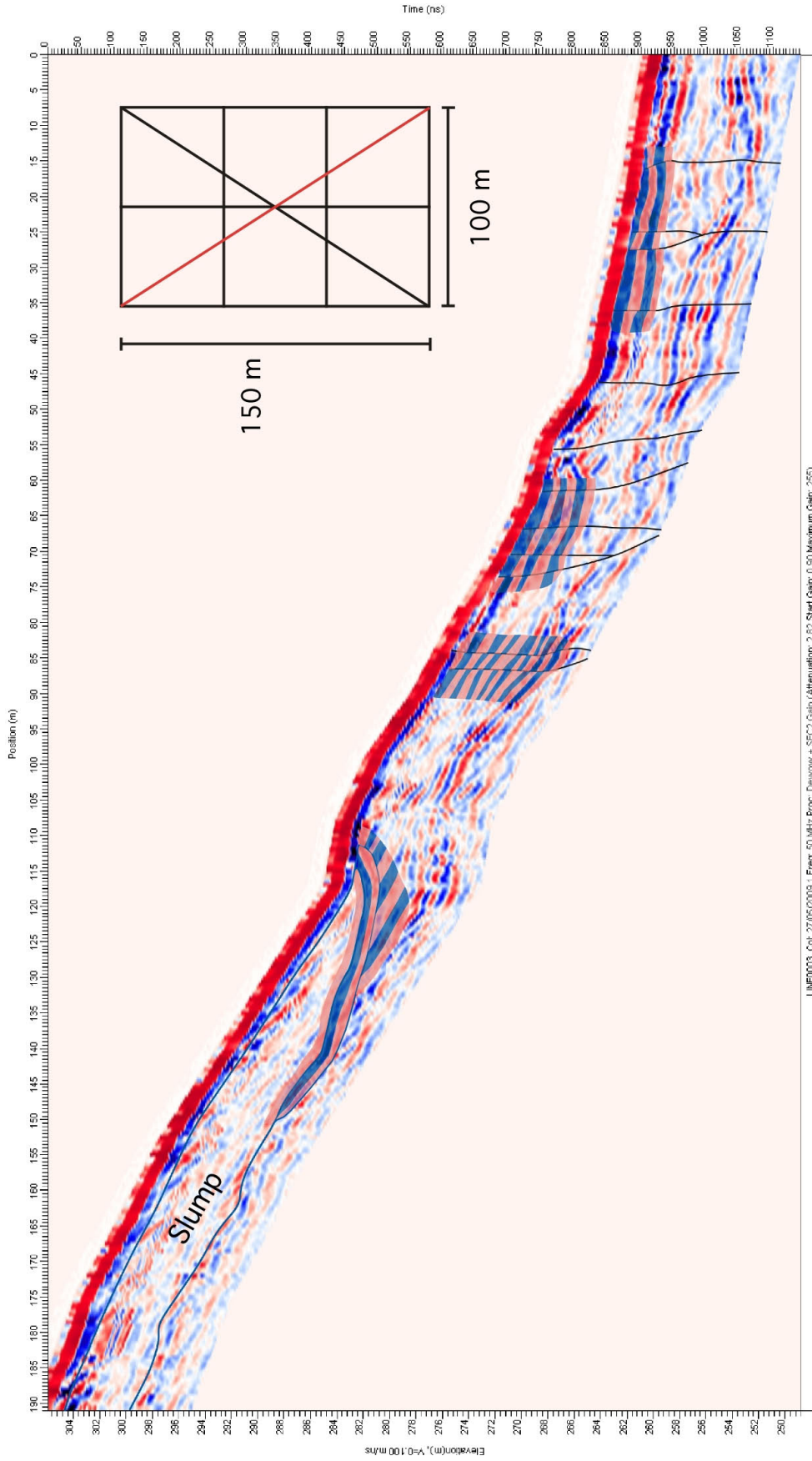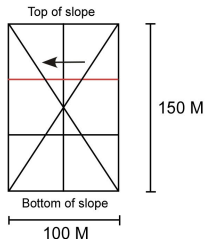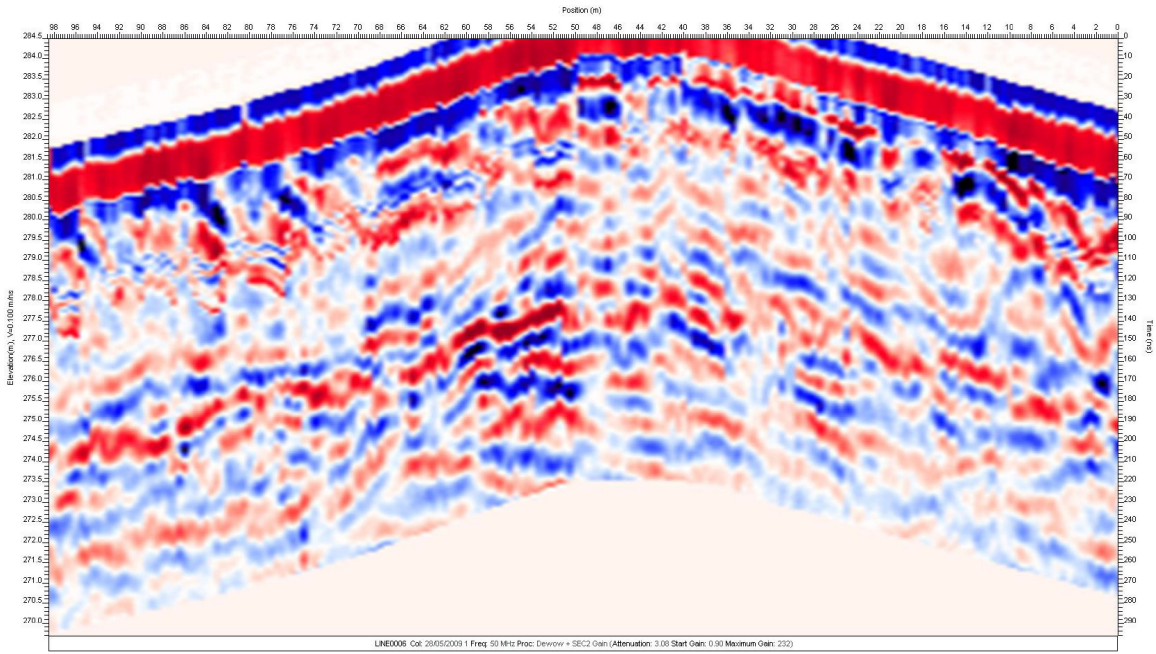
Figure 37. Site 1, 50 MHz, line 0006. This transect runs parallel to the fault across the alluvial fan and was used to help correlate elevations between perpendicular and diagonal transects. Faulting features are not apparent as this line does not cut across the fault. Red line on grid shows transect location.

does not quite reach the surface and has been buried beneath a thin layer of alluvium that has covered the entire alluvial fan.

This slump is ~75 m long and ~5 m thick along line 0000 (Figure 28) and becomes smaller through lines 0001 and 0002 (Figure 30 and 32). This would indicate the main portion of the slump is closer to the eastern side of the grid. The alluvial fan on which the grid was placed averages a fairly steep 30° from the top of the GPR grid to the base of the alluvial fan. Therefore, loose alluvial material sitting on this slope may be unstable in the event of movement in the area. Seismic activity along the fault, located directly below the alluvial fan, could have easily caused the failure of the slope, triggering the slump.

The transects taken parallel to the fault did not show any definite features associated with faulting as they did not cross the fault at a perpendicular angle, but were taken along strike of the fault (Figure 37). Any evidence for faulting in these transects would be a splay-type feature and travel through the lines in nearly the same direction as the line was taken, making it very difficult to recognize any definite faulting features. The parallel transects in the survey were not necessarily intended to help identify fault features, but were initially intended to help to visually correlate subsurface reflectors and elevations between the perpendicular and diagonal transects in order to create a 3-D image of the fault in the subsurface. This section of the study could not be completed as the final image desired could not be created with the geospatial computer programs available.

4.4 Interpretation of GPR Site 2

The 100 MHz antennas at site 2 also produced images that show many truncations of subsurface reflectors. Faults are interpreted in the same manner as on transects completed at site 1. Again, the grid was placed across an apparent fault scarp to ensure the presence of the fault in the subsurface. Similar to site 1, after viewing and analyzing the collected data, it is apparent that there are more fault splays in the subsurface than anticipated from the surface mapping. Offsets are discovered throughout the perpendicular transects and are not confined to the scarp itself.

The results of this GPR grid survey were compared to Kretzer's (2010) grid. Kretzer (2010) conducted a companion study and a similar survey, in which he imaged the same lines in the same locations using the 50 MHz antennas. There is an unmistakable difference when comparing the same transects completed with different antennas. As expected, the 100 MHz antennas produced much higher resolution images showing a higher number of continuous reflectors that are interpreted as sedimentary layers in the same depth window (Figure 38-40). Depth penetration, however, achieved by the 100 MHz antennas was only ~5 m compared to ~11 m for the 50 MHz antennas. The much higher resolution also revealed many more fault splays in the images produced by the 100 MHz antennas compared to images produced by the 50 MHz antennas. Line 0001 taken with the 100 MHz antennas revealed eighteen fault splays reaching the surface and only seven using the 50 MHz (Figure 38). Line 0002, the center transect, revealed sixteen fault splays reaching the surface with the 100 MHz antennas and only eight using the 50 MHz (Figure 39). The 100 MHz antennas revealed twenty-two fault splays reaching the surface in line 0004 while the 50 MHz had just ten (Figure 40). Interpretation of GPR lines undoubtedly differs from interpreter to interpreter and different numbers and locations of fault splays could be identified depending on the interpreter's knowledge and experience. However, it

is hard to imagine that this marked difference between the two sets of antennas is not truly the result of higher resolution of the existing subsurface geology.

As with site 1, the parallel transects completed for the grid at site 2 were taken in the same direction as the fault trend and do not show any immediate evidence for faulting. Any features related to faulting in the parallel transects would be very difficult to recognize as the direction of the fault would be nearly the same as the actual transect. Again at site 2, the parallel transects were not necessarily intended to identify fault features, but rather to help correlate subsurface reflectors and elevations across to each perpendicular transect (Figure 41).
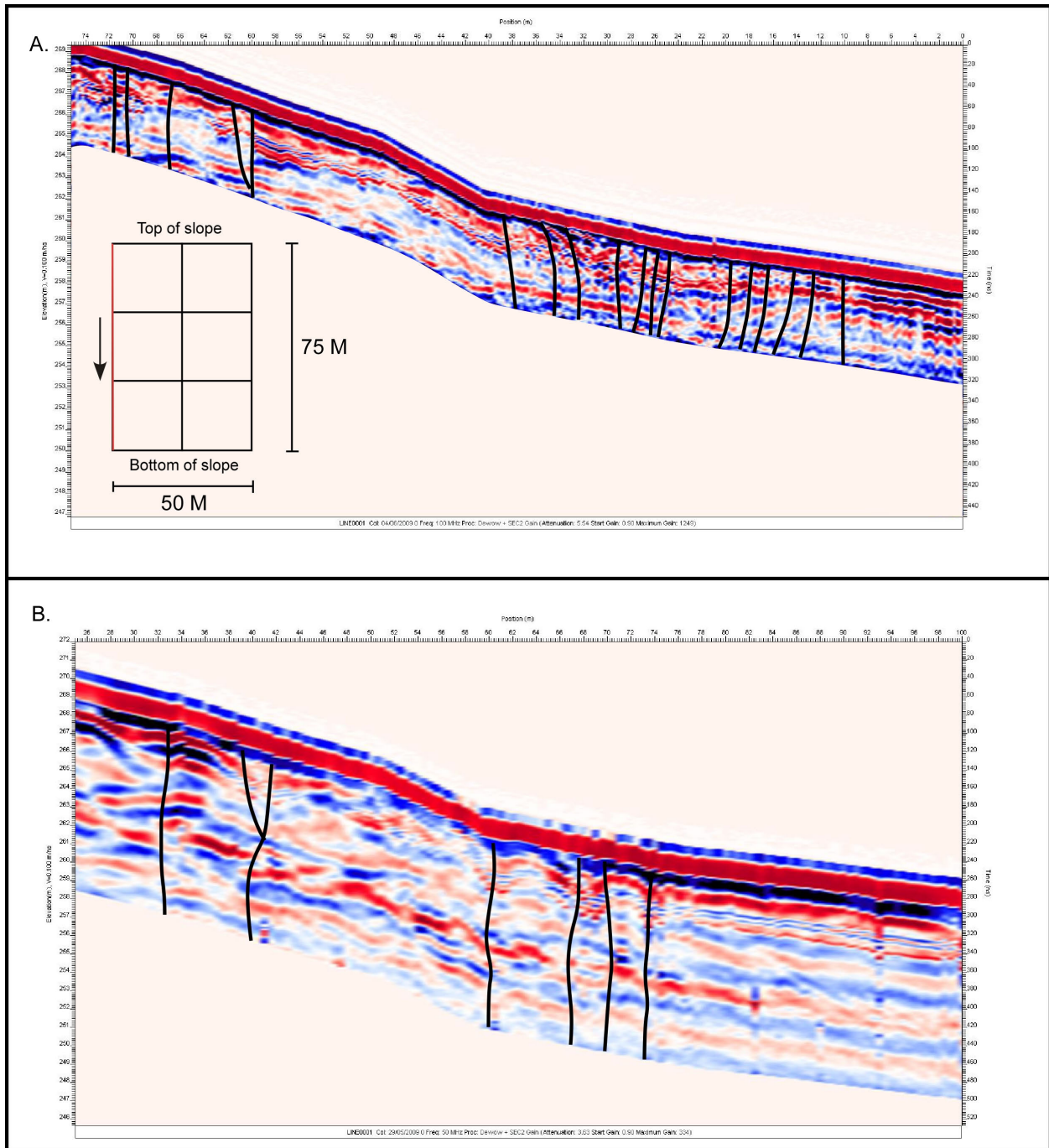
Figure 38. Site 2, Line 0001. 100 MHz transect (A) compared to 50 MHz transect (B) taken in the same location. Black lines represent inferred faults. Red line on grid shows transect location.
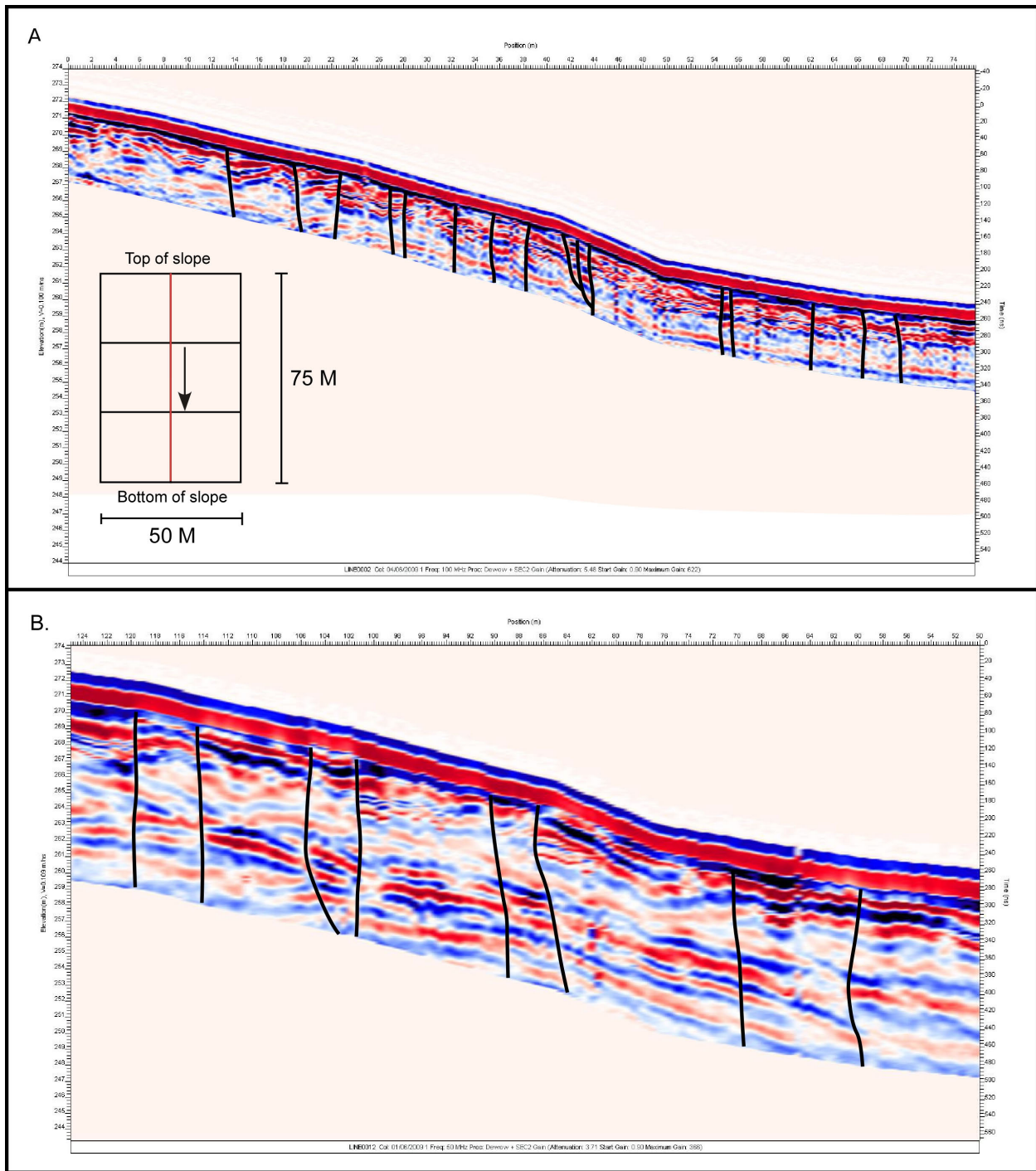
Figure 39. Site 2, Line 0002. 100 MHz transect (A) compared to 50 MHz transect (B) taken in the same location. Black lines represent inferred faults. Red line on grid shows transect location.
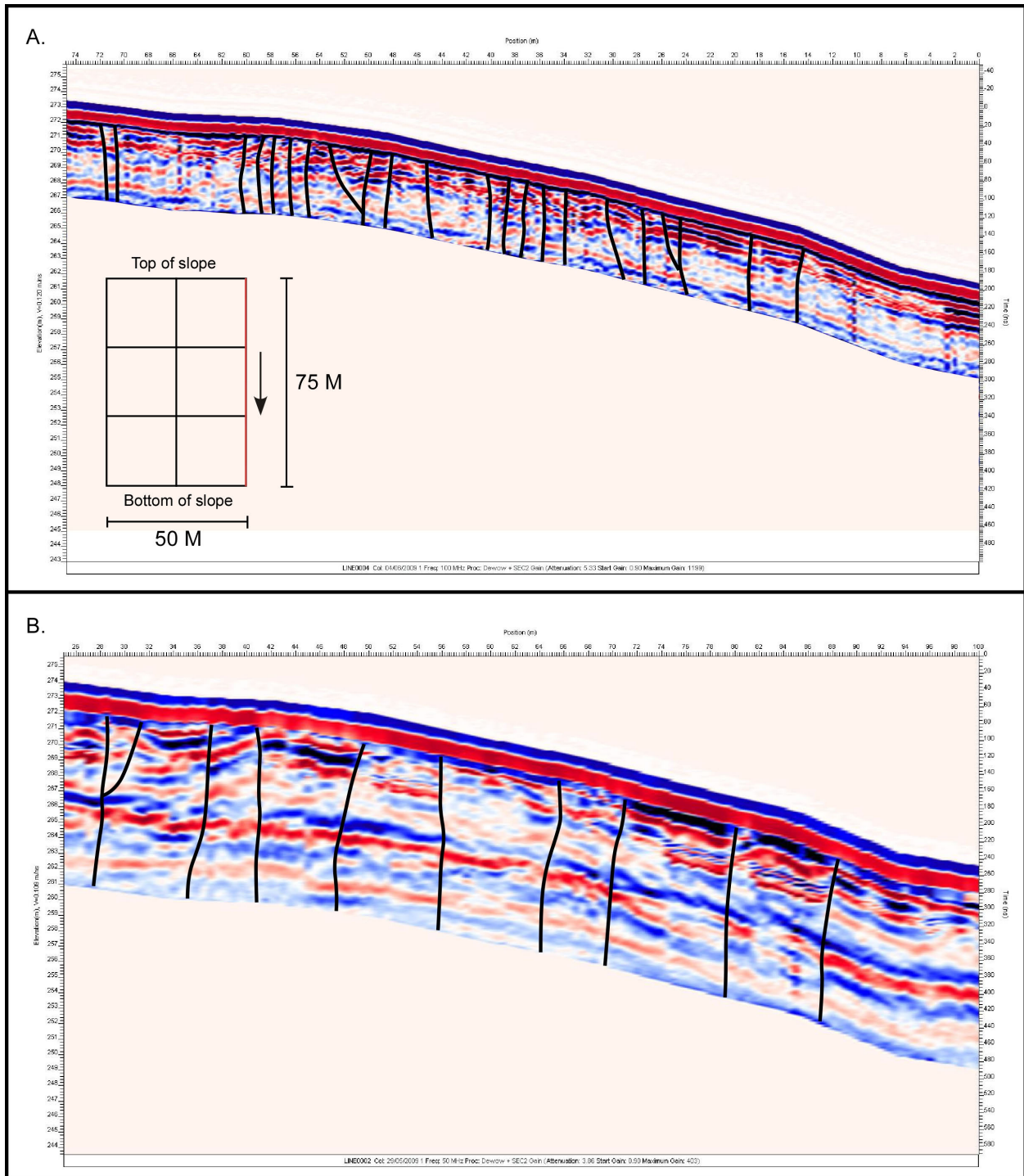
Figure 40. Site 2, Line 0004. 100 MHz transect (A) compared to 50 MHz transect (B) taken in the same location. Black lines represent inferred faults. Red line on grid shows transect location.
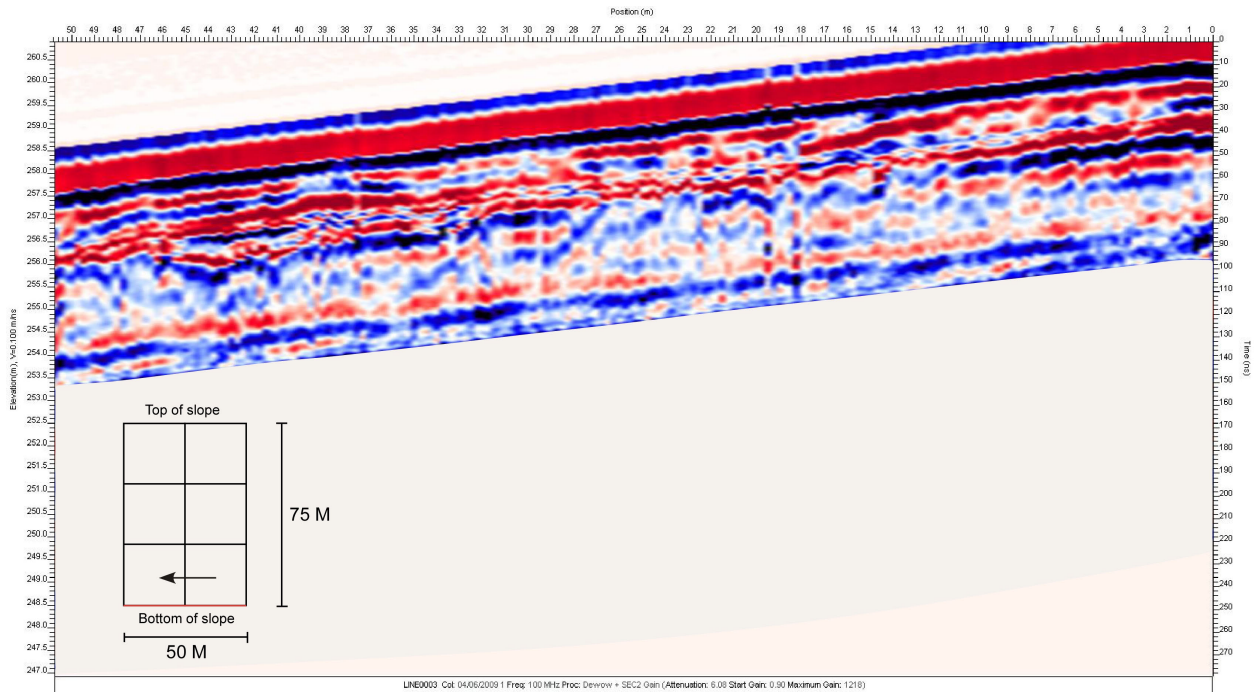
Figure 41. Site 2, 100 MHz. This transect runs parallel to the fault below the scarp and was collected with the intent to help correlate subsurface features and elevations between perpendicular transects. Faulting features are not apparent as this line does not cut across the fault. Red line on grid shows transect location.

Chapter 5: Discussion

5.1 Fault Geometry and Geomorphology

Two separate faults are identified and mapped in the field area; a subsidiary northern branch, and a southern branch that is interpreted as the more continuous, main fault. The northern branch is more difficult to identify in places and had fewer definite geomorphic features diagnostic of faulting. Although the general location of the northern fault can usually be found within the mapped area, in many places a layer of alluvium covers it with little geomorphic expression to pinpoint the exact location of the fault trace. As a result much of the fault trace is inferred. The southern, main branch of the fault is more easily identified in the field area as it passes through better-exposed Cretaceous volcanics at the surface and also passes along the Cerro los Alisos mountain front with more identifiable geomorphic features.

The southern branch was identified as the more active and prominent fault in the mapped area. However, to the east fault scarps along the northern fault become more pronounced and the northern branch appears to become the better developed feature, while the southern fault becomes less prominent with less geomorphic expression.. This suggests that the northern fault accommodates more of the motion to the east and begins to die out to the west. As the northern fault dies out, displacement is transferred to the southern fault, which accommodates most of the motion moving westward along the fault. This exchange of motion from the northern to southern fault creates a small step-over along the Agua Blanca fault.

Along GPR site 1, the grid was set up along a fault scarp surface to insure the subsurface images would cover a faulted area. The scarp was raised approximately 5 m on the northern side of the fault and suggests a normal component of motion to the fault, which agrees with conclusions reached by Schug (1987) and Madsen (2009). GPR transects at site one also

revealed a slight normal component of motion along fault splays where vertical movement could be identified. Site 2 also crossed a scarp raised ~3 m, where again a slight normal component of motion could be identified on fault splays in the subsurface.

5.2 Recognizing Strike-Slip Faults in the Shallow Subsurface

Others have successfully used GPR to image strike-slip faults (Cai *et al*., 1996; Yetton and Nobes, 1998; Slater and Niemi, 2003; Wallace and Nobes, 2009; Madsen, 2009). Knowing the principles of GPR and implications of the collected data, one can use the principles of structural geology and neotectonics to help guide in the interpretation of GPR profiles (Cai *et al*., 1996). Similar to other GPR studies, the faults and fault splays identified at GPR sites 1 and 2 are located and identified by apparent offsets in stratigraphy and not through direct reflections from the fault plane (Cai *et al*., 1996).

Although only one scarp at each location was readily visible at the surface to identify the fault trace, the GPR transects revealed many apparent fault splays that are not actually exposed at the surface. This lack of visible evidence is similar to observations by Madsen (2009), who documented the same observation in her GPR study.

A problem with recognizing truncations in the continuity of subsurface strata during strike-slip faulting is that a dip-slip component of offset could be very slight or non-existent. Each side of the fault may slide by the other, but with no or very little topographic change across the fault. Thus, the subsurface strata may remain at the same elevation and hide the actual fault plane. However, a strike-slip fault is hardly ever purely strike-slip in nature and is often accompanied by some amount of vertical offset (Sylvester, 1988). A slight normal component of slip was evident in many of the fault splays identified in the GPR grids agreeing with these past

studies. Even if motion along a fault is purely strike-slip, offsets in the strata can still be visible especially along alluvial fans such as in the study area. Alluvial fans deposit sediment parallel to earth's surface on an inclined and curved slope and, therefore, at slightly different elevations throughout the fan. As a result, even if there has been no vertical motion associated with the fault, strike-slip translation will lead to juxtaposition of different strata. This creates an apparent vertical offset along the fault and can be recognized in a GPR transect as the truncation and offset of strata in the subsurface.

5.3 Comparison between 50 MHz and 100 MHz Antennas

One of the more interesting findings at site 2 is that faults appear in the lower resolution 50 MHz transects that do not appear or do not correlate with faults in the higher resolution 100 MHz transects. It was expected to encounter faults in the 100 MHz transects that did not appear in the 50 MHz transects because the level of detail with the 100 MHz antennas is much greater and should consequently reveal more fault splays. However, finding faults in the 50 MHz transects that did not appear in the 100 MHz transects was unexpected. The reason may be the scale of observation of the antennas. The 100 MHz antennas reveal much more detail as evidenced by the larger number of apparent strata through the same depth appearing in the 100 MHz transects compared to the 50 MHz transects along the same line. However, the amount of detail revealed in the 100 MHz transects is much finer and small offsets of the stratigraphic layers by a larger number of near-vertical features may be interpreted as noise or unreliable and are, therefore, not interpreted as fault splays. The 50MHz antennas would not detect these details and the lower resolution images may suggest greater amounts of offset that is more readily interpreted as the expression of a fault surface.

Based on the GPR data collected, it is apparent that a greater number of faults are present in the subsurface than are actually identifiable at the surface. While some offsets in strata are obvious, others are only slight, which makes it possible not all features identified as faults are actually faults. To compensate for this, features used for the identification of faults were chosen consistently within an acceptable range. Others that are not continuous through multiple strata or offset in strata is too small to fully trace are left out.

Chapter 6: Conclusions and Implications

6.1 Conclusions

The geomorphology of the study area in the Valle Santo Tomas indicates that the Agua Blanca fault has been recently active. Many different geomorphologic features including deflected streams, shutter ridges, a pressure ridge, a sag pond, and scarplets reaffirm this conclusion. These geomorphic features are encountered in two separate zones, leading to the inference of a northern and southern fault in the study area. The faults are recognized along the surface through linear troughs and abrupt changes in topography along fault scarps. The conclusion that the fault has recently been active agrees with several past studies (Schug, 1987; Rockwell *et al*., 1993; Dixon *et al*., 2002).

Based on the GPR data, it is apparent that a greater number of fault splays exist in the shallow subsurface than evidenced at the surface. Although there is only one apparent scarp at the surface, fault splays are plentiful throughout the fault-perpendicular transects in both GPR grids. This suggests that the detailed structure of the Agua Blanca fault consists of a complex system of fault splays and that a main fault strand and several subsidiary splays exist in Valle Santo Tomas.

6.2 Implications for Future Studies

In order to have a better understanding of the Agua Blanca fault in its entirety, additional studies should be conducted farther to the east as similar studies have been performed previously to the west of the study area (Madsen, 2009). Farther east in Valle Santo Tomas or Valle Agua Blanca would be a logical progression for future study. Geomorphic mapping of the area and similar GPR work would be desirable and could help correlate with the present study and previous studies along the fault.

Depending on the scope and goals of a future study, GPR transects should be run using either the 50 MHz or 100 MHz antennas. A shallower, but more detailed transect results from using the 100 MHz antennas (although some large scale features may be lost) and could be used when a higher resolution image of the fault is desired or in the event a high water table creating interference is encountered. Overall, the 50 MHz antennas are found to be much more successful in achieving deeper penetration without losing too much resolution allowing the identification of major fault features. Also, rather than conducting time consuming transects parallel the fault that reveal relatively little about its nature, these could be omitted and instead only take GPS points along these lines to use later for elevation data connecting perpendicular transects. In this way more focus can be put on conducting more transects perpendicular to the fault so a greater area could be imaged. With this data combined into a geospatial program it may also be possible to create a 3-D model of the fault in the subsurface. This would help to see the subsurface orientation of the fault.

References

Allen, C.R., L. Silver, and F.G. Stehli, 1960. Agua Blanca fault, a major transverse structure of northern Baja California, Mexico. Geological Society of America Bulletin, vol. 71, p. 457-482.

Atwater, T.M., 1970. Implications of plate tectonics for the Cenozoic tectonic evolution of western North America. Geological Society of America Bulletin, vol. 81, p. 3513 - 3536.

Atwater, T.M., 1989. Plate tectonic history of the northeast Pacific and western North America. In *Geology of North America, Vol. N, Eastern Pacific Ocean and Hawaii*, edited by E.L. Winterer, D.M. Hussong and R.W. Decker, Geological Society of America, Boulder, CO, p. 21-72.

Atwater, T.M. and J. Stock, 1998. Pacific-North America plate tectonics of the Neogene southwestern United States: an update. International Geology Review, vol. 40, p. 375-402.

Cai, J., G.A McMechan, and M.A. Fisher, 1996. Application of ground-penetrating radar to investigation of near-surface fault properties in the San Francisco Bay region. Bulletin of the Seismological Society of America, vol. 86, p. 1459-1470.

Dickinson, W.R., 1996. Kinematics of transrotational tectonism in the California transverse ranges and its contribution to cumulative slip along the San Andreas transform fault system. Geological Society of America Special Paper 305, Boulder, CO, p. 1-46.

Dickinson, W.R., M. Ducea, L.I. Rosenberg, H.G. Greene, S.A. Graham, J.C. Clark, G.E. Weber, S. Kidder, W.G. Ernst, and E.E. Brabb, 2005. Net dextral slip, Neogene San Gregorio – Hosgri fault zone, coastal California: Geologic evidence and tectonic implications. Geological Society of America Special Paper 391, Boulder, CO. p. 1-43.

Dixon, T., J. Decaix, F. Farina, K. Furlong, R. Malservisi, R. Bennett, F. Suarez-Vidal, J. Fletcher, and J. Lee, 2002. Seismic cycle and rheological effects on estimation of present-day slip rates for the Agua Blanca and San Miguel-Vallecitos faults, northern Baja California, Mexico. Journal of Geophysical Research, vol. 107, p. ETG 5-1 to 5-23.

Gary, M., R. McAfee, and C. L. Wolf, 1974. *Glossary of Geology*: American Geological Institute, Washington, D.C.

Gastil, R.G., G.J. Morgan, and D. Krummenacher, 1981. Tectonic History of Peninsular California and Adjacent Mexico. In *Rubey Volume No.1, The Tectonic Development of California*, edited by G. Ernst, Freeman Press, San Francisco, CA, p. 284-306.

Hatch, M.G., 1987. Neotectonics of the Agua Blanca Fault, Valle Agua Blanca, Baja California, Mexico. [M.S. Thesis]: San Diego State University, San Diego CA

Herzig, C.T., 1991. Petrogenetic and tectonic development of the Santiago Peak Volcanics, northern Santa Ana Mountains, California. [Ph.D. dissertation]: University of California. Riverside, California.

Irwin, W.P., 1990. Geology and plate-tectonic development. In *The San Andreas fault system, California*, edited by R.E. Wallace. U.S. Geological Survey Professional Paper 1515. p. 61-77.

Kearey, P., K.A. Klepeis, and F.J. Vine, 2009. Global Tectonics. Third Edition. Wiley-Blackwell, Hoboken, NJ.

Kretzer, C., 2010. Geologic Mapping and Ground-Penetrating Radar Surveys of the Valle Santo Tomas Segment of the Agua Blanca Fault, Baja California, Mexico. [M.S. Thesis]: Texas Christian University.

Madsen, S.R., 2009. Geomorphic Mapping and Ground-Penetrating Radar Survey of the Western

    Segment of the Agua Blanca Fault, Baja California, Mexico. [M.S. Thesis]: Texas Christian

    University.

Moore, D.G., 1969. Reflection profiling studies of the California Continental Borderland – 2.

    structure and Quaternary turbidite basins. Geological Society of America Special Paper no. 2.

    Boulder, CO. p. 107-142.

EKKO-for-DVL pulseEKKO 100 User's Guide. Sensors and Software Inc., 2005.

Rockwell, T.K., M.E. Hatch, and D.L. Schug, 1987. Late Quaternary rates - The Agua Blanca

    and Borderland Faults. Final Technical Report, US Geological Survey contract no. 14-08-

    0001-22012. p. 1-122

Rockwell, T.K., D.L. Schug, and M.E. Hatch, 1993. Late Quaternary slip rates along the Agua

    Blanca fault, Baja California, Mexico. In *Geological investigations of Baja California: South*

    coast geological society, annual field trip guidebook, edited by P.L. Abbott, no. 21, p. 53-92.

Schug, D.L., 1987. Neotectonics of the Western Reach of the Agua Blanca Fault, Baja

    California, Mexico. [M.S. Thesis]: San Diego State University, San Diego CA

Slater, L. and T. Niemi, 2003. Ground-penetrating radar investigation of active faults along the

    Dead Sea transform and implications for seismic hazards within the city of Aqaba, Jordan.

    Tectonophysics, vol. 368, p. 33-50.

Stock, J. and P. Molnar, 1988. Uncertainties and implications of the late Cretaceous and Tertiary

    position of North America relative to the Farallon, Kula, and Pacific plates. Tectonics, vol. 7,

    p. 1339-1384.

Suarez-Vidal, R., G. Armijo, P. Morgan, R. Bodon, and G. Gastil, 1991. Framework of recent

    and active faulting in northern Baja California. In *Gulf and peninsular province of the*

Californias, edited by J. Dauphin and B. Simoneit, American Association of Petroleum Geologists Memoir 47, p. 285-300.

Sylvester, A.G., 1988. Strike slip faults. Geological Society of America Bulletin, vol. 100, p. 1666-1703.

Tischler, M., M.E. Collins, and S. Grunwald, 2002. Integration of Ground-Penetrating Radar Data, Global Positioning Systems, and Geographic Information Systems to Create Three-Dimensional Soil Models. International conference on ground penetrating radar, vol. 4758, p. 313-316.

Wallace, S.C., D.C. Nobes, K.J. Davis, D.W., Burbank, A. White, 2010. Three-dimensional GPR imaging of the Benmore anticline and step-over of the Ostler Fault, South Island, New Zealand. Geophysical Journal International, vol. 180, p. 465-474.

Wesnousky, S., 2005. The San Andreas and Walker Lane fault systems, western North America: transpression, transtension, cumulative slip and the structural evolution of a major transform plate boundary. Journal of Structural Geology, vol. 27, p. 1505-1512.

Yetton, M.D., and D.C. Nobes, 1998. Recent vertical offset and near-surface structure of the Alpine fault in Westland, New Zealand, from ground penetrating radar profiling. New Zealand Journal of Geology and Geophysics, vol. 41, p. 485-492.

Geospatial References Used

Instituto Nacional de Estadista y Geografia, 1996, Rodolfo Sanchez Taboada Topographic Map, San Juan, Mexico, Instituto Nacional de Estadista y Geografia.

Software Used

ACD Systems, Inc., 2005, Canvas with GIS: Version 10.6.3, Victoria, BC, Canada, ACD

Systems, Inc.

Environmental Systems Research Institute, Inc. (ESRI), 2006, ArcMap: Version 9.2. Redlands,

CA, Environmental Systems Research Institute, Inc. (ESRI).

Environmental Systems Research Institute, Inc. (ESRI), 2006, ArcCatalog: Version 9.2.

Redlands, CA, Environmental Systems Research Institute, Inc. (ESRI).

Sensors & Software, Inc., 2009, EKKO_View Deluxe: Version 1.4. Mississauga, ON, Canada,

Sensors & Software, Inc.

Sensors & Software, Inc., 2009, EKKO_View 2: Version 2.1. Mississauga, ON, Canada, Sensors

& Software, Inc.

Appendix

The appendix shows the rest of the GPR lines that were taken parallel to the main fault. They were originally intended to help correlate features form one perpendicular transect to the next in an attempt to create a 3-D image of the subsurface. This attempt was unsuccessful, but parallel transects were still useful in linking elevations across the grids.
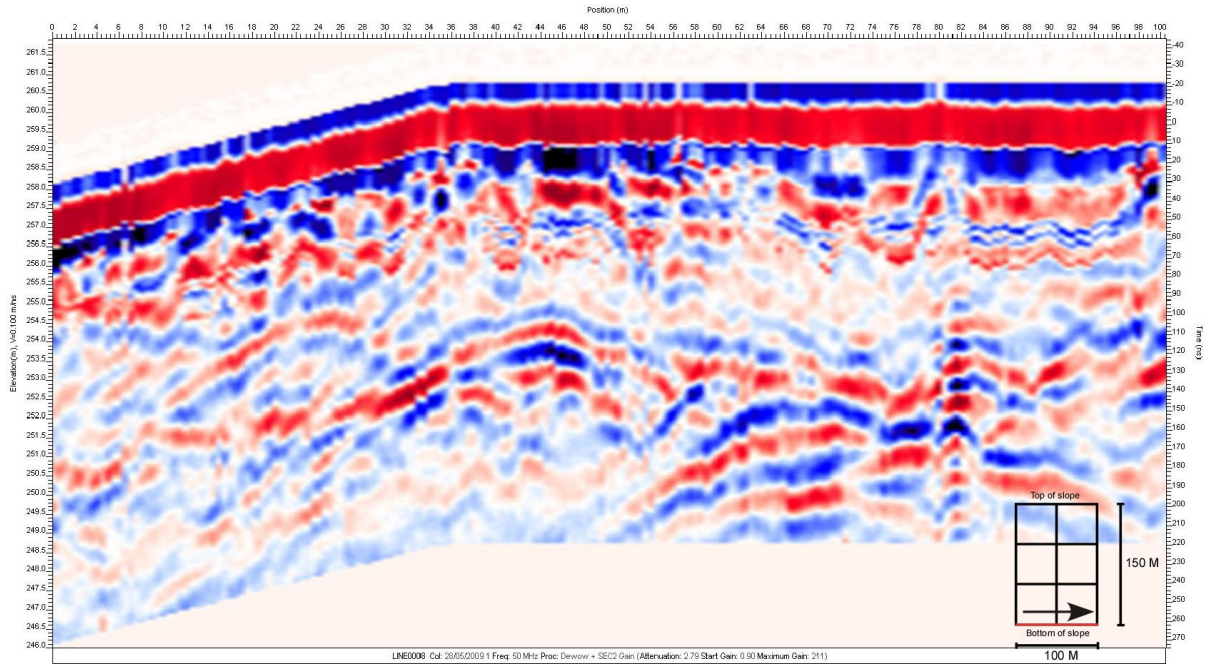
Additional Parallel Transects From Site 1
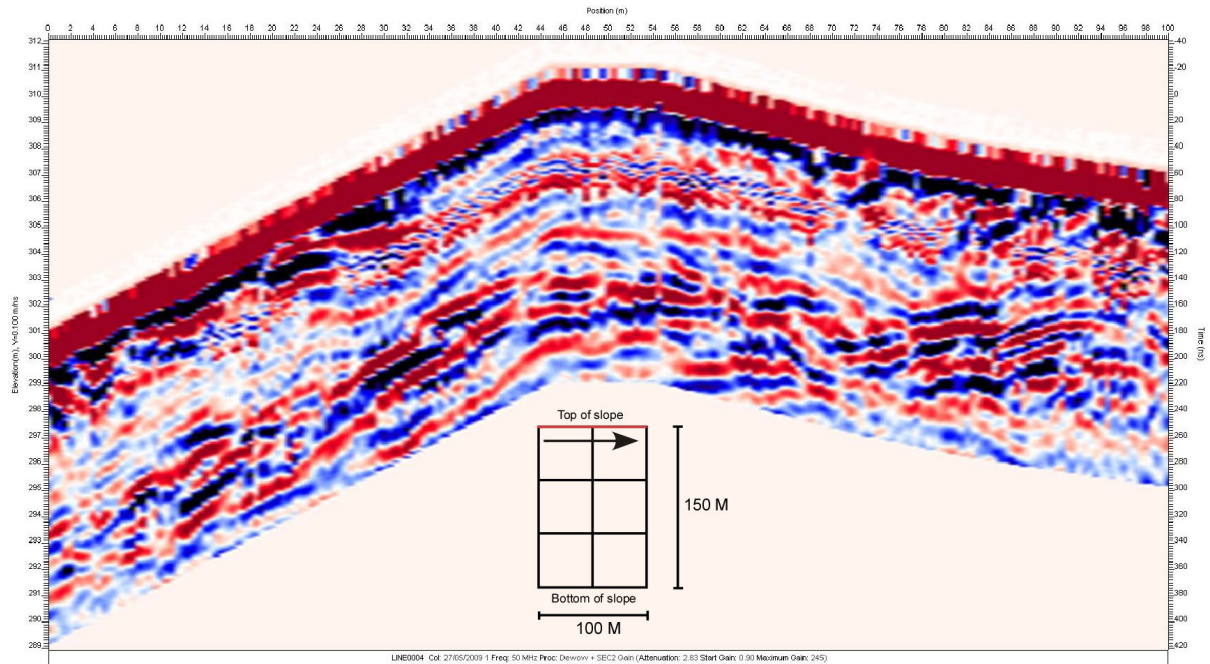
Appendix Figure 1. Site 1, Line0004, 50 MHz. Additional parallel transect used in the study. Red line on grid shows transect location and arrow indicates direction the line was taken in.
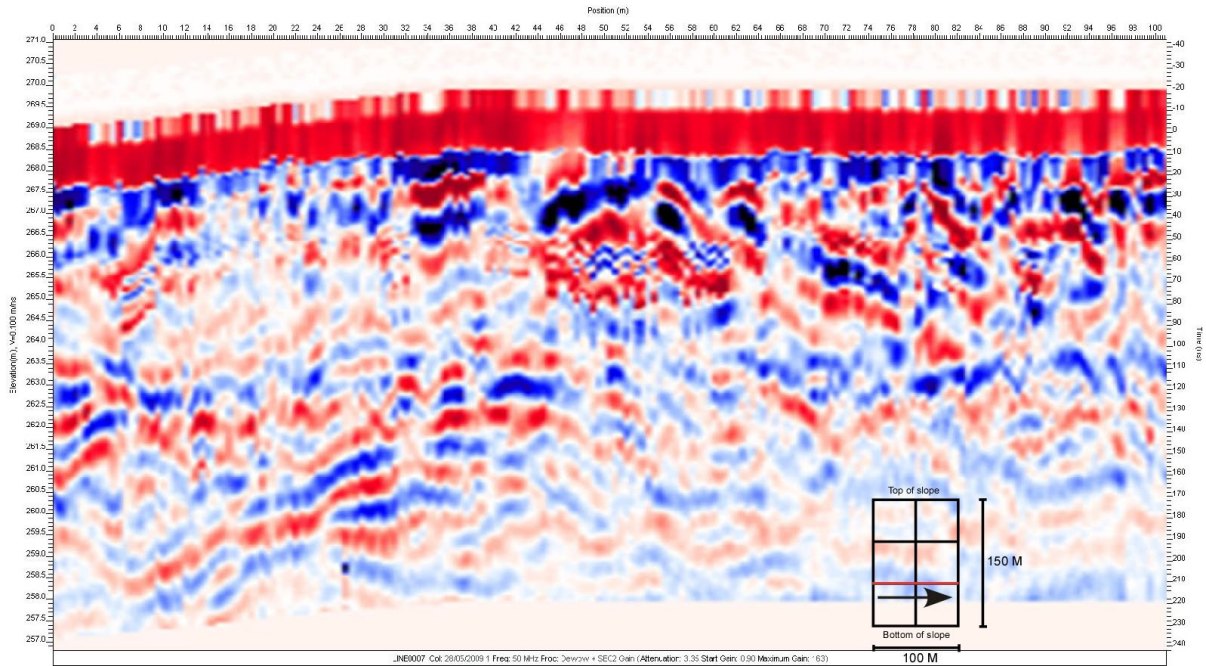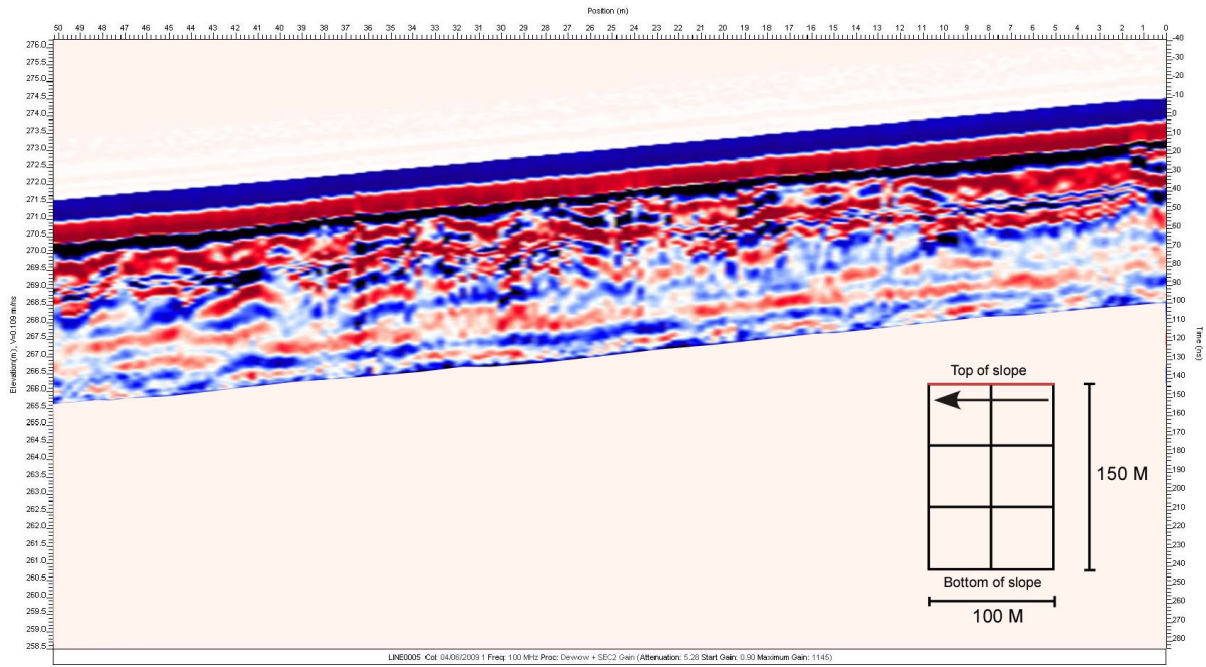
Appendix Figure 2. Site 1, Line0007, 50 MHz. Additional parallel transect used in the study. Red line on grid shows transect location and arrow indicates direction the line was taken in.

Appendix Figure 3. Site 1, Line0008, 50 MHz. Additional parallel transect used in the study. Red line on grid shows transect location and arrow indicates direction the line was taken in.

Additional Parallel Transects From Site 2

Appendix Figure 4. Site 2, Line0005, 100 MHz. Additional parallel transect used in the study. Red line on grid shows transect location and arrow indicates direction the line was taken in.
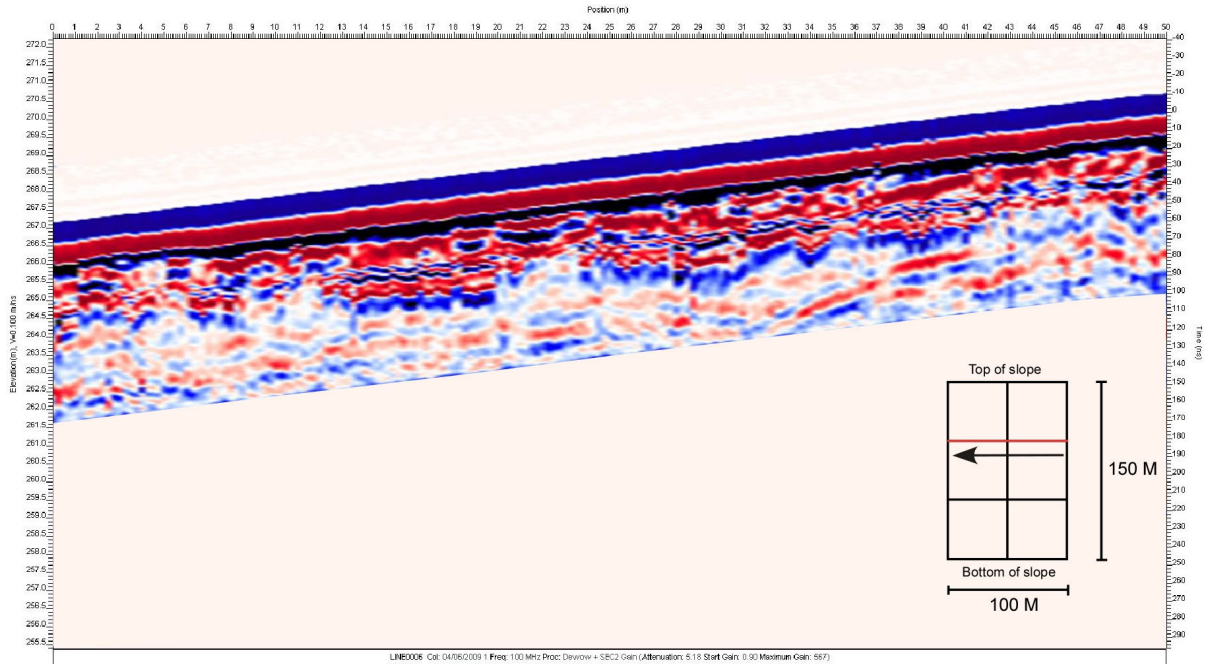
Appendix Figure 5. Site 2, Line0006, 100 MHz. Additional parallel transect used in the study. Red line on grid shows transect location and arrow indicates direction the line was taken in.
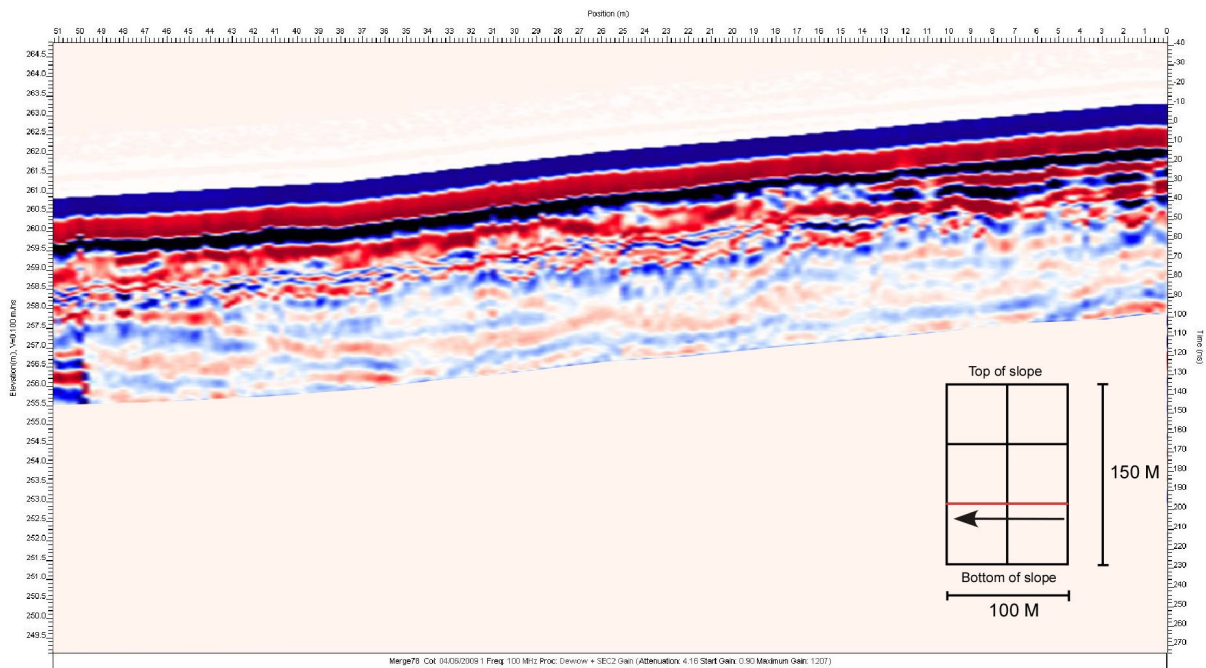
Appendix Figure 6. Site 2, Merged Line78, 100 MHz. Additional parallel transect used in the study. Red line on grid shows transect location and arrow indicates direction the line was taken in.

Vita

Personal   William Rainey Cage

Background   Falfurrias, Texas

Born   June 21, 1985, San Antonio, Texas

Parents   Presnall and Stephanie Cage

Education   Bachelor of Science in Environmental Earth Resources, Minor in

        Business, Texas Christian University, Fort Worth, Texas, August 2008

        Master of Science, Geology, Texas Christian University, Fort Worth,

        Texas, August 2010

Abstract

Geomorphic Mapping and Ground-Penetrating Radar Survey of the Agua Blanca Fault in Valle de Santo Tomas, Baja California, Mexico

By William Rainey Cage, M.S., 2010
Department of Geology
Texas Christian University

Dr. Helge Alsleben – Assistant Professor of Geology

The Agua Blanca fault is interpreted as an active, dextral strike-slip fault in northern Baja California about 100 km south from the U.S.-Mexico border. Tectonically, the Agua Blanca fault is associated with the San Andreas fault system, which comprises the main portion of the transform plate boundary between the Pacific and North American plates. Although there are estimated slip rates for the fault, there is no recorded seismicity. Geomorphic maps at a scale of ~ 1:5,000 were completed within the Valle Santo Tomas. Features characteristic of strike-slip faulting such as deflected streams and shutter ridges suggest the fault is still active and should not be considered abandoned. Ground-penetrating radar surveys were conducted in order to image the fault in the near surface. Based on the GPR data, it is apparent that a greater number of fault splays exist in the shallow subsurface than evidenced at the surface. This suggests that the detailed structure of the Agua Blanca fault consists of a complex system of fault splays and that a main fault strand and several subsidiary faults splays exist in Valle Santo Tomas.